TALLINN UNIVERSITY OF TECHNOLOGY

FACULTY OF CHEMICAL AND MATERIALS TECHNOLOGY

DEPARTMENT OF MATERIAL SCIENCE

The template-assisted wet-combustion synthesis of mesoporous core-shell structured materials.

Master Thesis

Nikhil Kumar Kamboj

Supervisor: **Prof. Irina Hussainova**

Co- supervisor: **Marina Aghayan**

Materials and Processes of Sustainable Energetics

Tallinn 2016

Declaration

Hereby I declare that this master thesis is my original investigation and achievement, submitted for the master degree at Tallinn University of Technology has not been submitted for any degree or examination.

Nikhil Kumar Kamboj

TALLINNA TEHNIKAÜLIKOOL

KEEMIA- JA MATERJALITEHNOLOOGIA TEADUSKOND

Materjaliteaduse instituut

Mudel-abistatud märg-põlemise meetodil mesopoorsete kärgmaterjalide süntees

Magistritöö

Nikhil Kumar Kamboj

Juhendaja**: Prof. Irina Hussainova**

Kaasjuhendaja: **Marina Aghayan**

Materjalid ja protsessid jätkusuutlikus energeetikas

Tallinn 2016

CONTENTS

ABBREVIATIONS AND ACRONYMS

ANF – Alumina nanofiber

EDS - Energy dispersive spectroscopy

1D- one dimensional

DTA - Differential thermal analysis

DSC - diffraction scanning calorimetry

SEM – Scanning electron microscope

TEM – Transmission electron microscope

TG - Thermogravimetric

TM - Transition metal

XRD – X-ray diffraction

wt.% – Weight percentage

SCS – Solution Combustion Synthesis

SHS - Self-propagating High temperature Synthesis

VC S – Volume Combustion Synthesis

1. INTRODUCTION

The extensive growth of the population of the world challenges to create new materials with enhanced functionality and lifetime expectancy [1]. The state-of-art in research today involves development of new methods to design and create "exotic" materials in the form of nanoparticles, nanofibers, nanolayered structures, bulk monolithic, single-/poly-crystalline, glassy, composites, and cellular structures. Another challenge is to study the morphology properly, characterize the properties and compute process-structure and structure-property correlations.

Recent advances in research on 1D nanostructures indicates that, specially nanofibers have wide range of predefined properties and are widely applied as catalyst support (a high aspect ratio combined with a large surface area), bio-sensors, membranes, and nanofillers for advanced composites. Materials with one-dimensional (1D) nanostructure are preferred building blocks for catalytic nano-architecture, and can be used to fabricate designed catalysts [31], as well as, in turning dielectric materials electrically conductive (typically with carbon nanotubes). In many cases it is favorable to have a continuous network of fibers, which, however, cannot be achieved using current nanofibers. Typical length of nanofibers produced nowadays is between 100 nm to 100 μm. This means that they can be used as a dispersion of discrete fibers of bundles in matrix material. Additionally, there is a problem of nanoparticles agglomerating within the matrix material that gives weak points to the resulting matrix. Longer fibers can be arranged into a continuous network which will significantly improve the mechanical properties of matrix material. This continuous network could be formed either by nonwoven (e.g. by wet-laying; needle punching or similar) or woven techniques. The latter expects the ability to spin nanofibers into yarns which is not possible in the case of short nanofibers. Such self-standing nanofiber structures would combine good properties of nanofibers (e.g. high strength, high surface area) with good properties of textile materials (e.g. flexibility, tear resistance).

In the thesis, one such material, a mesoporous network of alumina nanofibers, was used as a precursor to prepare a range of nanocomposites, mainly $NiO-Al_2O_3$, $NiO-MgO-Al_2O_3$, $NiO-CeO_2-Al_2O_3$ and $Fe_2O_3-Al_2O_3$, which could open new doors of application. Utilizing the specific properties of alumina nanofibers, a macro-mesoporous nanocomposite, which consist of an aligned fibrous nanocomposite was synthesised via wet-combustion method, recently developed in Tallinn University of Technology. This method is combination of sol-gel, dip

coating and combustion synthesis method. Thus, the mesoporous network of alumina nanofibers was wetted by a reactive solution containing the metal precursor and organic fuel, followed by the heat treatment until self-ignition and combustion-synthesis of the desired material. The organic fuel can act as metal dispersing and complexing agent, and provide homogeneous distribution of metal precursors throughout the mesoporous network. After heating the wetted specimen at $400^{\circ}C$, ignition of combustion in the nanopours mesoporosity of the bundles of fibers takes place in a short time (timescale of seconds) and large amount of gases evolve leading to the synthesis of nanometric materials with unique properties without further calcination. In particular, the wet-combustion synthesis enables to synthesise-deposit wide range of materials and their morphology can be studied in single-step and cost-effective way.

In this work, the mechanism of the wet-combustion process as well as the effect of the fuel type and amount on the composition and morphology of the combustion product of the mentioned system is thoroughly studied by various characterization methods which include XRD, SEM-EDS, magnetic properties, DTA/TG and pyrometer techniques.

2.   REVIEW OF LITERATURE

2.1   Properties and applications of alumina

Aluminum oxide (Al_2O_3) or alumina is one of the most important ceramic material that is widely used in many technological applications such as electrical insulators, catalyst supports [2,3] filters, abrasive and thermal wear coatings, etc. Alumina exists in many metastable forms (transition aluminas), such as γ-, δ-, η-, θ-, κ- phases and thermodynamically stable α-Al_2O_3 phase, which is the only stable form at any pressure and temperature [3].

The transition aluminas are derived by thermal dehydration of aluminum hydroxide precursors. (Fig.1) The transformation of the boehmite to γ-Al_2O_3 is of particular interest as γ-Al_2O_3 is regarded as the most important transition in alumina. The γ-Al_2O_3 is one of the most important catalytic support due to large surface area, high catalytic activity, however, it transforms rapidly to α-Al_2O_3, accompanied by loss of porosity and specific surface area.
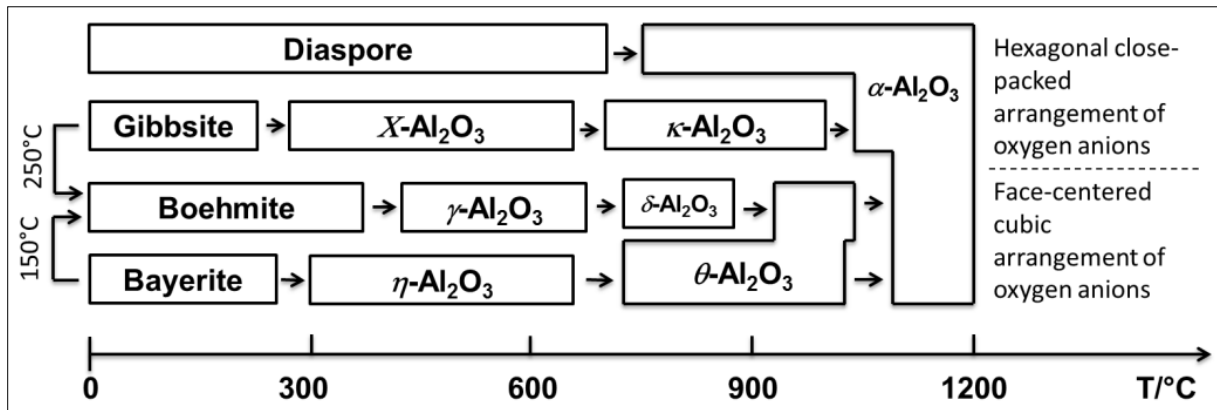
Figure 1 *Phase transitions of metastable aluminum polymorphs towards the formation of α-Al₂O₃ (adapted from ref [8]).*

Thus, an understanding of the structures of polymorphs of alumina would therefore be of great importance. γ-Al$_2$O$_3$ is estimated to have a defect cubic spinel structure in Fig.2 (a). The unit cell of the spinel, Mg$_8$[Al$_{16}$]O$_{32}$, is formed by a cubic close stacking of 32 oxygen atoms, 16 aluminum atoms occupying one-half of the available interstices, and 8 magnesium atoms in tetrahedral holes. γ- Al$_2$O$_3$ (Al$_8$[Al$_{(40/3)}\square_{(8/3)}$]O$_{32}$) has aluminum cations distributed over the octahedral and tetrahedral interstitial sites defined by the oxygen anion sub lattice [5]. The 8/3 cation vacancies ($\square$) per cubic unit cell are attributed to the octahedral sites to satisfy the correct stoichiometry of aluminum oxide. This leads to the cation vacancies of Al^{3+} vacancy defect sites and the hollow structure of γ-Al$_2$O$_3$ [6].

By annealing γ-Al$_2$O$_3$ transforms to α-Al$_2$O$_3$ in Fig 2(b) via δ and θ-Al$_2$O$_3$. The transition temperatures between metastable aluminas into stable α-Al$_2$O$_3$ (oxygen atoms form a hcp packing of spheres where 2/3 of the octahedral vacancies are occupied by aluminum atoms) are varied with the particle size, defect density and presence of seeds [7].
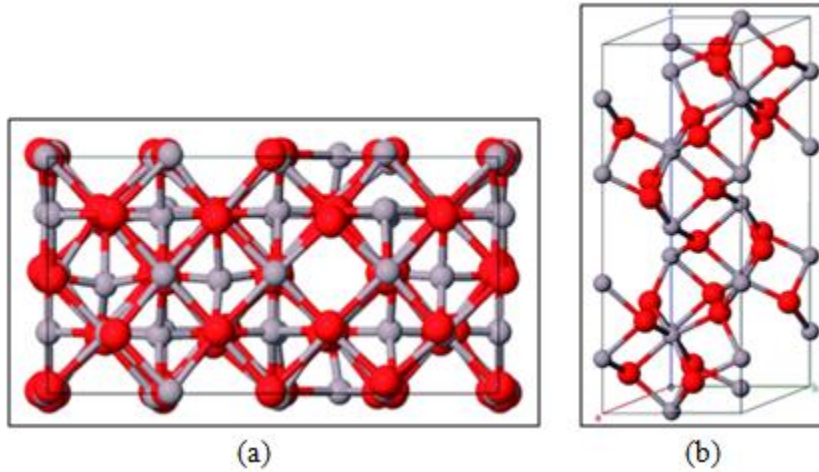
Figure 2 *The structure of (a) γ-Al₂O₃ and (b) α-Al₂O₃ with color code (Al grey and O red) (Ref [4]).*

In particular, the particle size of alumina nanoparticles has been identified as one of the crucial factors controlling the relative stability of γ-Al$_2$O$_3$. The defective metastable aluminas with smaller particle size have higher surface energy. An alumina polymorph with lower surface energy becomes more stable than one with higher surface energy as the particle size decreases (i.e., the surface area increases). However, the phase transformation from γ- to α-Al$_2$O$_3$ is accompanied by dramatic loss of surface area (Table 1)

Table 1 *Represents the polymorphs of alumina with Specific Surface Area (Ref [7]).*

Polymorphs of Alumina	Specific surface Area(SSA)
γ-Al$_2$O$_3$	179 m^2/g – 497 m^2/g
δ-Al$_2$O$_3$	156 m^2/g – 230 m^2/g
θ-Al$_2$O$_3$	11 m^2/g – 200 m^2/g
α-Al$_2$O$_3$	2 m^2/g – 17 m^2/g

The applications of alumina are numerous. Alumina is used as a catalyst due to its textural properties, such as surface area, good design in dust free pneumatic loading and low abrasion for dust formation. High macroporosity provides excellent catalytic activity and pore size distribution [9-11]. Alumina catalysts are considered as the most effective components for methane steam reforming [26]. Various polymorphs of alumina are investigated for using

alumina as a catalyst. Most of commercial supports in the industry focus on γ-Al_2O_3 in α-Al_2O_3 co-precipitated or in impregnated catalysts form.

Alumina is also used as a catalytic support. Properties important for determining the activities of catalyst support are surface area, crystallite size, pore size, and pore size distribution and in literature Al_2O_3 is regarded as the best catalyst support [12]. Study by Ganley J.C et al [13] concluded that alumina as a support on metal catalyst nickel, increases the catalyst dispersion by factors around 2 to 3.

Thus the polymorphs of alumina have different physical properties (e.g. density, dielectric constant, energy gap, acid-base properties, etc) from each other and have different applications. The κ-Al_2O_3 finds its application in surface coating of cutting tools because of its extreme hardness [15]. Due to high surface area and porosity [16] of γ-Al_2O_3 it is used as a catalytic support and promoter in the catalyst industry [17].

2.2 The unique properties of alumina nanofibers.

Nanofibers possess different unique properties compared to the microscale fibers made of the same material. Recently, the synthesis and application of one-dimensional (1D) nanomaterials including nanofibers, nanowires, nanorods, and nanotubes have attracted great attention because of unique and enhanced properties [18, 19, 86], which make them potential materials for the next generation nano-devices and emerging applications which are illustrated in Fig.3.

Amongst the 1D nanomaterial, alumina nanofibers have drawn tremendous attention. Alumina nanofibers are reported to have high strength, excellent chemical stability, low thermal conductivity, good electrical insulation and are prone towards corrosion resistance

Apart from that, alumina nanofibers possess ultimate tensile strength and enormous specific surface area combined with nanoscale fiber diameter. Superior tensile strength is attributed to the purity in crystal structure where tensile strength is quite close to the theoretical value of the inter-atomic bond strength. Such fibers would be very attractive reinforcement materials in all sorts of composite materials, but especially in ceramic and metal matrix composites where polymer fibers cannot be used due to high processing temperatures that polymers cannot withstand. The super high aspect ratio of nanofibers can form a continuous network that is productive in stopping crack propagation in fragile ceramic matrix, for example. Compared to microscale reinforcement fibers the weight fraction of nanofibers is considerably smaller making the resulting composite lighter [20]. This is

especially important in transportation applications (e.g. ceramic brakes, bearings and other components) [86]. Another important parameter of nanomaterials is surface area which is much larger compared to larger particles due to the small diameter of fibers and the increased number of fibers per unit volume.

The alumina nanofibers, developed in Estonia, combines large surface area, surface properties of γ-alumina, and high chemical purity, which makes them an excellent choice for catalyst and filtering applications. Nanoscale fiber diameter has a potential to considerably reduce diffusive resistances in catalytic systems ensuring better accessibility to catalytic sites therefore enhancing catalyst efficiency [21-23]. Alumina nanofibers act as a precursor for building structured catalysts.

Nanofibers with high aspect ratio are favorable also, considering health and safety risks. Compared to typical nanotubes and other nanoparticles, nanofibers of high aspect ratio form larger agglomerates so that it prevents from the danger of inhalation or skin penetration, for example, is considerably smaller than in the case of conventional nano-size particles [86]. Webster et al. [24] proved that alumina nanofibers are promising materials for orthopedic applications, their in vitro study to determine osteoblast functions (specifically, adhesion, alkaline phosphatase activity and ability to deposit calcium) on alumina nanofibers of various crystalline phases was commendable.

Interest in alumina nanofibers as membranes increases intensively, compared with the conventional membranes, alumina nanofibers enable to filter out viruses and waterborne pathogens from the blood. Moreover, they are resistive towards crack propagation [25]. Alumina nanofibers membranes are also used for enhancing hemodialysis [14].

Figure 3 *Represents the potential applications of alumina nanofibers.*

2.2.1   Fabrication of alumina nanofibers

Combination of the mentioned unique properties of alumina nanofibers, opens wide range of advanced applications. However, in practice, the use of nanofibers in ceramic composites and catalyst systems is not very well established, because of the high price of the existed functional nanofibers, final product of the production techniques, which would allow to obtain functional nanofibers in an industrial scale in a cost effective way.

Nevertheless, there are different techniques used for alumina nanofiber production. Alumina nanofibers were synthesized by hydrothermal synthesis, which resulted in rod-like

nanofibers with diameter of 15-20 nm and aspect ratios of 10 to 20 (300 nm to 400 nm long) [26]. Sol-gel technique allowed to synthesis fibers with 2 nm in diameter and 70 nm in length [20]. Zhu et al. [32] obtained γ-alumina nanofibers from aluminium hydrate with poly (ethylene oxide) surfactant and has the potential application to be used as a catalyst. Both hydrothermal and sol-gel processes include the hydrolysis of starting aluminium compound, aging of the sol over 24 hours. Typical factors influencing the quality of resulting fibers depends on many aspects including: the nature of the starting material, whether a surfactant or templating agent is used, the amount of water used, the aging time in the hydrolysis, the pH value of the reaction mixture, and the hydrothermal temperature. Hence such processes are complicated and time consuming. Moreover, usually, after those processes calcination is needed which requires keeping nanofiber precursors at elevated temperature (typically ranging from 500 up to 1200 ^{0}C) for several (typically from 1 to 5 h) hours depending on the calcinations temperature. This can result in agglomeration and control over size of the product. Non-crystalline alumina nanofibers were prepared by flame aerosol method of 2–10 nm in diameter and 20– 210 nm in length [27]. Mercury mediated method was used to fabricate well aligned amorphous fibers with diameters of 5-15 nm and length of several μm [28]. Crystalline nanowires of size around 50 nm in diameter and around 2 μm in length were synthesized by vapor-liquid-solid process [29].

Electrospinning is a recently developed, widely used technique, which enables to achieve long (up to several centimeters) alumina nanofibers with diameters ranging from 20 to 1000 nm [30]. Though long nanofibers can be produced by electrospinning this technique has some serious drawbacks. Electrospun fibers are produced as a coating rather than bulk fibers. Resulting fibers often form a crosslinked network and are therefore difficult or impossible to separate and process further.

In this work we used alumina nanofibers, developed in Estonia, in which formation method is based on growing alumina nanofibers directly from the melt of liquid aluminium. Fibers growth takes place at the interface of melt aluminum and ambient atmosphere. The analysis has demonstrated that fibers with diameter of 7∓2 nm and maximum length of bundles up to 15 mm can be produced.

2.3   Nanocomposites based on alumina nanofibers.

Currently nanoscale additives have been studied for enhancing several properties of matrix materials. The alumina nanocomposites are regarded as very important ceramic

engineering material [33] not only because of the well-known properties of corrosion-erosion-resistant material but also possibilities of improving these nanocomposites due to its relatively cost than other materials. Many researchers have proven that nanofibers enable to enhance mechanical properties of ceramic composites better than traditional nanoparticles. To date, alumina matrix reinforced with SiC fiber have been reported to have potential applications in the high stress area of the heat engines, where good thermal shock properties are required. Alumina matrix reinforced with SiC laid the foundation of the composites of alumina-mullite and alumina-zirconia materials. These composites share the same applications as of alumina-SiC composite material [34].

Zirconia toughened alumina was obtained with the ANF whiskers thoroughly dispersed into zirconia matrix, at temperatures ranging from 1000 to 1200 °C, with the help of the spark plasma sintering technique [35]. It was concluded that Al_2O_3-ZrO_2 nanofiber composite has toughness values is three times higher and strength value two times higher than the conventional alumina [36]. To improve the refractoriness and crystalline stability of alumina and silicate fibers Glaushkin et al. added Cr_2O_3 to the fibers [37].

The significant improvements in mechanical and electrical properties of alumina nanofibers by adding graphene which acts like a support proved by Aghayan et al [38]. Alumina nanofibers supports as a nanocomposite for the stabilization of various catalysts by intervening the metal cluster. For instance, Pt catalyst supported on the alumina nanofibers produces hydrogen from sugars and alcohol [39].

The open porous structure, large surface area makes the nanofibrous alumina an indispensable material for support for active nanoparticles. Alumina nanofibers have been used as supports for stabilizing metal cluster in various catalytic applications. In this case, large average pore diameters decrease the resistance to interior diffusion, minimising the diffusion control of chemical reactions. Alumina nanofibers were proved to be good support of nanoscale catalysts for Fischer-Tropsch refining processes [40]. It was clearly demonstrated that large surface area of the alumina nanofibers favors the dispersion of the cobalt nanoparticles. Shen et al. [41] prepared rod like, thermally stable spinel of Zn-Al complex oxide using alumina nanofibers with Zn ion. The synthesized composite material acted as environment friendly catalyst for the reduction of NO. The composite catalyst of microsilica and alumina nanofibers was proved to be promising materials for capturing tar or soot from diesel catalytic converters [42].

The nanofibers enable to enhance mechanical properties of ceramic composites better than individual composite. Hence, most of the production of the high-alumina composites today finds its applications in fabrication of high temperature refractory material and many more.

2.4 Synthesis of nanocomposites

The realization of unique physical properties of nanostructure composites depends critically on the morphology (size and shape) and homogeneity of the components. Numerous recent efforts have been directed towards the fabrication of nanocomposites to enhance their performance in currently existing applications and to open new prospective areas of applications. A viable approach to synthesize functionalized composite materials consists of colloidal deposition developed by Shutilov et al [43]. They combined various techniques which includes wet impregnation, chemical vapor deposition, deposition precipitation, etc. Usually wet-chemical methods are followed by long thermal treatment at elevated temperature [44], which often leads to the agglomeration of the deposited particles and their broad size distribution.

Preparation of highly dispersed nanoparticles uniformly distributed over the nanostructured template is an actual challenge. Recently, Feng et al. [45] developed a novel sol-flame method to fabricate one-dimensional nanocomposites. This method includes preparation of solution of metal salt, which coats uniformly the as-prepared nanowires by dip-coating. Afterwards, the metal salt-coated nanowires are annealed over a flame for a few seconds. As a result, nanowires are coated by metal oxides. Due to the high flame temperature and short annealing time, nanoscale particles form around the nanowires.

Aghayan et al. [38] covered alumina nanofibers by graphene layers by catalyst-free one-step chemical vapor deposition (CVD) process.

Another possibility to synthesize nanocomposites is combustion synthesis which provides high flash temperature at short time. The high temperature provides the decomposition of the precursors. However, the short duration of the process prevents surface diffusion of metal species and, therefore, their agglomeration and sintering [46].

A template-assisted wet-combustion method based on sol-gel, dip coating and combustion synthesis is developed by our group [47, 48 and 49] to fabricate various composite nanofibers in a controllable combustion mode in one step.

In this work, wet-combustion method was used to fabricate nanoscale composite materials. So the effective combination of dip coating and solution combustion prepare nanostructures in a simple, controllable and cost-effective way. This method includes the preparation of a relative solution containing metal(s) salt(s) and fuel(s). The obtained reactive solution of metal nitrate and fuels are doped onto the network of the mesoporous template and heated to ignite the combustion process. A second scale combustion takes place in the mesoporous structure of the template, which leads to the formation of the nanosized particles. A large amount of gases release during the combustion process provides fast cooling of the sample. The morphology and chemical composition of the obtained product can be controlled by optimizing the initial parameters of wet-combustion method.

2.5   Objectives

The overall objective of the research work is to functionalize, optimize and produce mesoporous materials consisting of composite core-shell structured nanofibers. The thesis work is aimed to produce fibrous structures for catalysts support substrates and magnets by recently developed template-assisted wet-combustion method represented a combination of sol-gel, dip coating and combustion synthesis, which was recently developed and patented by team of supervisors.

To meet the research goals, the following sub-goals are underlined:

• To develop an approach for homogeneous deposition of a metal oxide onto alumina nanofibers keeping highly aligned structure of the network.

• To study the influence of conditions such as fuel type, fuel-to oxidizer ratio, etc. on the development of tailored structure.

• To study the morphology and thermal stability of the product.

• To study the magnetic properties of the Fe_2O_3-ANF nanocomposites.

3. EXPERIMENTAL AND MATERIALS

3.1 Designing the system

Alumina nanofibers with a single fiber diameter of 7 ± 2 nm and length of 5-7 cm were functionalized by four different metal oxides (NiO, MgO, CeO_2, Fe_2O_3) by the wet-combustion synthesis approach. Metal nitrates as source of metal ion act as oxidizers and different organic fuels (glycine, urea and citric acid) as source of energy and reducers used for the combustion are dissolved in distilled water to prepare reactive solutions (Table 2). The reactive solutions were soaked by the mesoporous network of fibrous alumina. After aging and homogeneously distribution of the reactive solution, it spread all over the alumina network. The specimen was heated until 400° C for 30 minutes in a muffle furnace, where the combustion took place (Fig..4).

Table 2 *Constituents for composites fibers processing.*

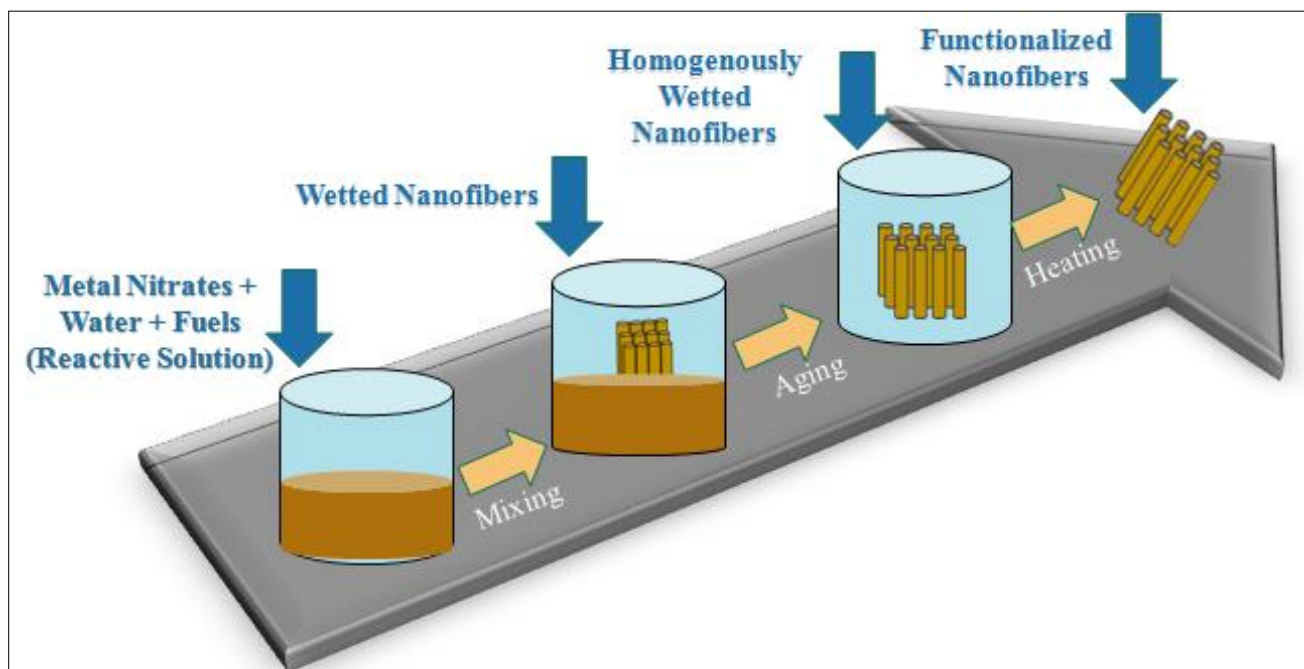| Compound	Purity	Supplier
$Fe(NO_3)_3*9H_2O$	>95	Merck
$Mg(NO_3)_2*6H_2O$	>99	Sigma-Aldrich
$Ni(NO_3)_2*6H_2O$	≥98.5	Sigma-Aldrich
$Ce(NO_3)_3*6H_2O$	≥98	Sigma-Aldrich
Glycine	≥99	Sigma
Urea	>99	Sigma-Aldrich
Citric acid	≥99.5	Sigma-Aldrich

Figure 4 *Schematic representation of functionalization of alumina nanofibers.*

3.2 Characterization Techniques

Phase and microstructural analysis were carried out by using X-ray diffraction (XRD), scanning electron microscopy (SEM). The mechanism of the combustion process was investigated by using different in situ thermal techniques, including thermogravimetric analysis (TGA) and pyrometric analyses.

3.2.1 X-ray Diffraction

XRD technique is a rapid analytical technique for studying chemical composition of a material, their crystal structure, crystallite size and atomic spacing [51]. X-rays emitted from a tube are directed at the material where its electrons collide with the photons from the incident beam causing diffractions. These beams are diffracted at many angles due to the many crystalline planes present in the material according to Bragg's law (eq 1).

$$n\lambda = 2d\sin\theta \tag{1}$$

Where n is an integer, λ is the wavelength of incident wave, d represents distance between the planes in the atomic lattice, and θ is the angle between the scattered planes and

incident ray. The data from the measured intensity and diffraction angles, the average crystallite size of the material can be calculated using the Scherrer (eq 2):

$$D = K.\lambda/B.\cos\theta \qquad (2)$$

Where D is mean size of crystalline in nm , which may be smaller or equal to the grain size. K is a coefficient with a value of 0.9. λ is the X-ray wavelength. B is the line broadening at half the maximum intensity (FWHM). This quantity is also denoted as (2θ). θ is the Bragg angle.

In this study, powder X-ray diffraction (Philips PW3830 X-ray Generator) measurements were performed within the angle range $2\theta = 20 - 70°$ with a step size of 0.02° and a count time of 0.4 s, using Cu Kα radiation ($\lambda = 0.154056$ nm) with a working voltage and current of 40 kV and 100 mA, respectively.

3.2.2 Scanning electron microscopy

Scanning electron microscope is a technique for the characterization of materials which produces image by scanning it with a focused beam of electrons. The versatility of SEM analysis is derived from large measure of the rich variety of interactions that a beam electron undergoes in a specimen.

Elastic scattering events affects the trajectories of the beam of the electrons inside the specimen without altering the kinetic energy of the electron. Elastic scattering is responsible for the phenomenon of electron backscattering that forms important signal in SEM. Inelastic scattering occurs due to the transfer of energy from beam of electrons to the atoms of the specimen leading to the generation of secondary electrons (Auger electrons) [52].

In this study, scanning electron microscopy (SEM Zeiss EVO MA 15, Germany) equipped with EDS (energy dispersive X-ray spectrometer) with voltage of up to 20 kV and magnifications up to 50 kX and was used for examination of the precursor materials and the functionalized final product. The samples were coated with gold before examination. The morphology of the material was also investigated by JEOL 2100F transmission electron microscope (HRTEM) operating at 200KV and equipped with a field emission electron gun providing a point resolution of 0.19 nm. The microscope was coupled with an EDS (INCA x-sight, Oxford Instruments).

3.2.3 In-situ Thermal Analysis

3.2.3.1   Differential thermal analysis and Thermogravimetric analysis

Thermal gravimetric analysis (TGA) is a method of thermal analysis in which changes in physical and chemical properties of materials are measured as a function of increasing temperature (with constant heating rate), or as a function of time (with constant temperature and/or constant mass loss). A plot of mass percentage against temperature can enable the interpretation of mass loss curve transformations.

Various physical and chemical methods affect the curve characteristics of DTA/TG. Physical factors include adsorption (exothermic), desorption (endothermic), change in crystal structure (endo or exothermic), crystallization (exothermic), melting (endothermic), vaporization (endothermic), and sublimation (endothermic). Chemical factors which affects the curve are oxidation (exothermic), reduction (endothermic), break down reactions (endo or exothermic), chemisorption (exothermic), and solid state reactions (endo or exothermic) [85].

The kinetics of the process were studied with simultaneous coupled thermal analysis (TG-DSC) with STA449C "Jupiter" (Netzsch Gerätebau GmbH. Experiments were performed in synthetic dry air (21% O_2, balance nitrogen; Linde AGA) flow of 20 ml/min with heating and cooling rates of 10°C/min.

3.2.3.2   Pyrometric analysis

Pyrometer, a type of infrared thermometer has an optical system and detector. The parameter that is taken by the optical system into account is thermal radiation onto the detector. Hence the related equation for the output signal works on thermal radiation of the target object j, the constant of proportionality σ, called the Stefan-Boltzmann constant and the emissivity ε of the object given by the (eq 3).

$$j = \varepsilon.\ \sigma.\ T^4 \tag{3}$$

Hence, temperature-time history of the synthesis process is recorded by highly accurate MPAC IGAR 12-LO Digital 2-color pyrometers with fiber optic and a response time of 2ms. The pyrometer measures in the 2-color principle (ratio principle) in which two adjacent wavelengths are used to calculate the temperature in the range from 499 up to 2200 ^{o}C.

3.2.4 Magnetic Properties

Magnestism is the physical phenomena of magnetic fields. The material can be mostly classified into broad catagories of ferromagnetic, ferrimagnetic, paramagnetic and antiferromagnetic. The magnetic property of the material depends on various factors like temperature and other factors like pressure and applied magnetic fields. In this work, investigation of magnetic measurements of ferrites (maghemite) at low temperatures were carried out with Quantum Design SQUID-VSM dc magnetometers and at 300 K using Microsense EV 7 VSM.

4   RESULTS AND DISCUSSION

4.1   Characterization of pristine alumina nanofibers

One-dimensional nanostructures possess "exotic" properties. Moreover, the properties of a material, even with a well-defined composition, are highly depended on its morphology, crystalline structure and microstructure of the polymorph.

The structure of the network of pristine alumina nanofibers Fig. 6(a) are studied by XRD Fig. 5, SEM (Fig. 6(b,c)) and nitrogen adsorption Fig. 6(d) techniques.

XRD pattern of pristine alumina nanofibers is depicted in Fig. 5. The diffraction lines of ANFs can be indexed to a cubic structure with space group Fd-3m (a=7.8400 Å). It was reported that the morphology of γ-alumina nanofibers remained unchanged up to about 1200 °C and transformation γ→α transformation occurred at temperatures above 1200 °C [63]. Heat treatment of ANFs over 1200°C resulted in a stable α-alumina polymorph. Alumina transformations from metastable aluminas to α-Al_2O_3 by conversions can be given by $Al_2QO_{3-v/2}$ $(OH)_v$ $\theta_{1-v/2}$, where Al represents the aluminum ions, Q is cationic vacancy in divalent sites, OH the hydroxyl groups substituting the oxygen in the normal positions of the anionic sublattice, θ is anionic vacancies of spinel structures, and v ranges from (0≤v≤2) [57].
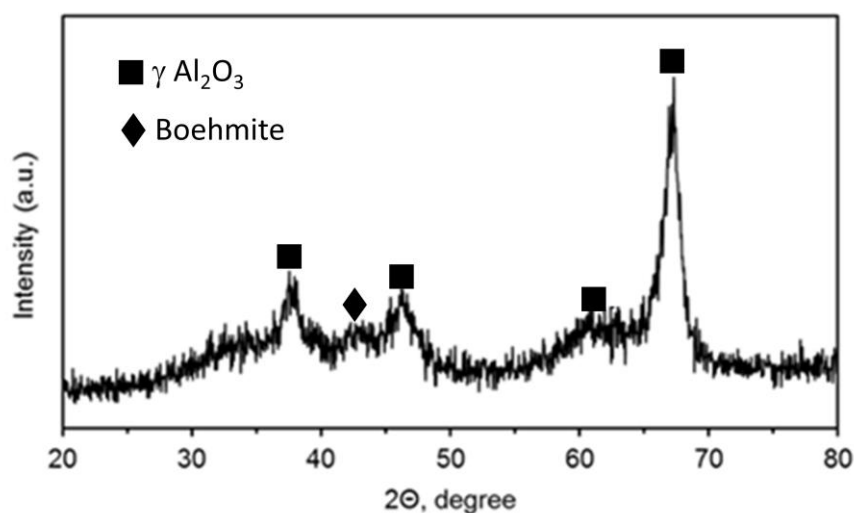

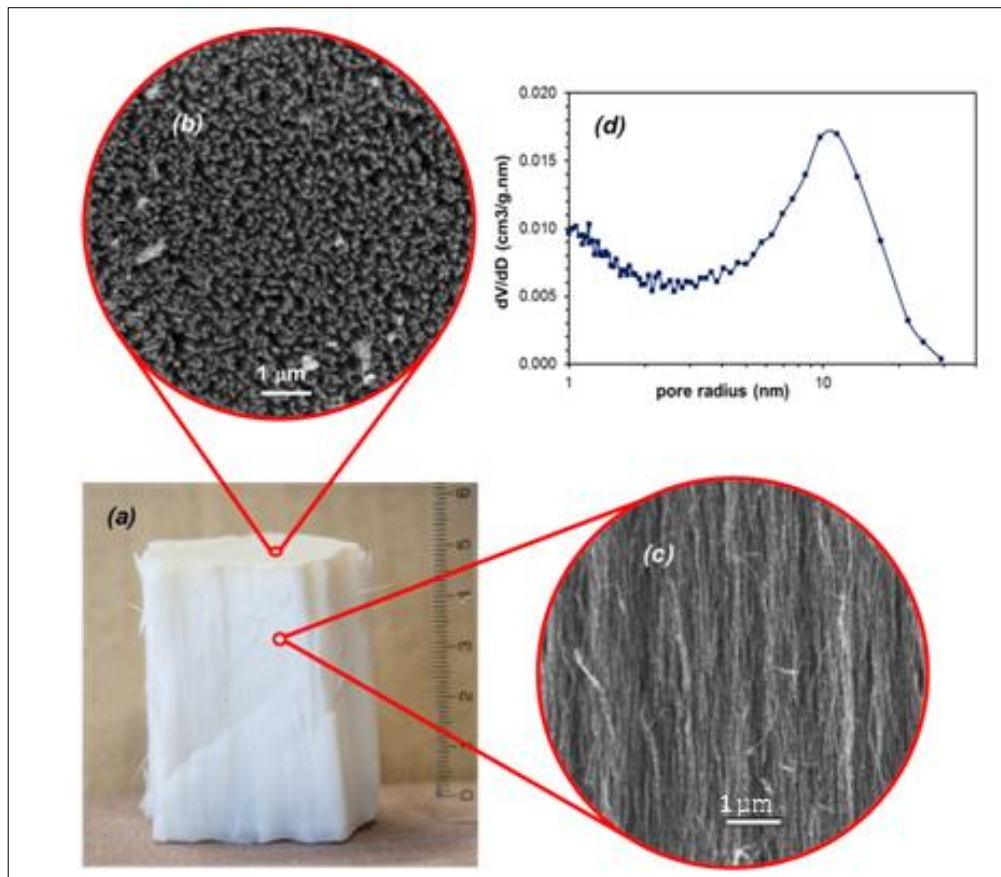**Figure 5** *X-ray diffraction pattern of pure ANF sample.*

Figure 6 *The network of ANFs (a) SEM micrographs of (b) top and (c) side views, (d) differential pore size distribution of ANFs.*

The nitrogen adsorption isotherms of the network of ANFs showed pore size distribution around 10 nm in Fig. 6(d). The large pore radius is one of significant property of alumina nanofibers, which is contributed due to the fact that, presence of inter-fibrous voids in randomly stacked alumina nanofibers. It can be seen from Fig. 6(d), pore radius of the alumina nanofibers exhibited an extremely broad distribution, because the pore structure resulting from the randomly stacking of fibrous nanoparticles are close to a three dimensional network, and do not possess regular shape and size [31, 58]. Figure 7, depicts the model of pristine alumina nanofiber. Model advocates that ANF contains some bonded water which can be a possibility to deposit different compound on the surface of the fibers.
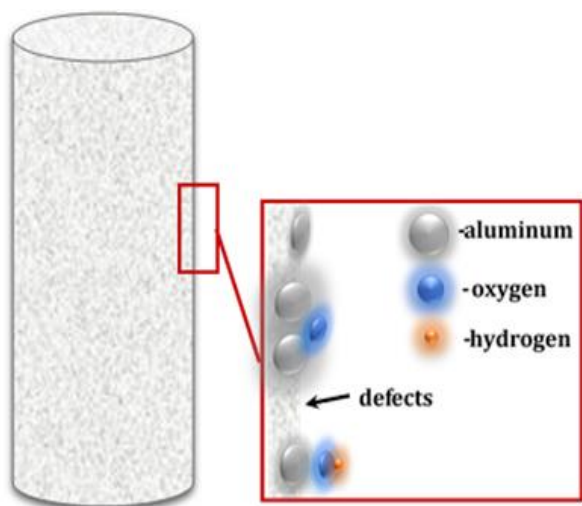
Figure 7 *Model of pristine alumina nanofiber.*

4.2 Nickel oxide based nanocomposites

Alumina-supported nickel catalyst is an important catalyst in various industrial processes. However, after a certain period, depending on the operating conditions, destructive effects such as coking, poisoning, sintering leads to the deactivation of the catalysts [50]. Many researchers report that carbon deposition and sintering can be depressed using highly dispersed active Ni sites [55]. A way of improving the dispersity of nickel sites is formation of $NiAl_2O_4$ spinel, which is reported to have a good effect on the suppression of carbon deposition [60]. Another option to enhance the dispersivity of nickel is to use mixed oxides along with nickel oxide. Seok et al [65] studied the influence of five different oxides on the catalytic behavior of nickel for methane dry reforming. The highest CO_2 conversion on the Al_2O_3 supported catalyst was reported to be of the following order of activity: Ni/MgO> Ni/ZrO_2 > Ni/CeO_2 > Ni/La_2O_3 > Ni/MnO and $Ni/MnAl_2O_4$. MgO and CeO_2 can be the potential promoters that can enhance the activity of Ni/Al_2O_3. CeO_2 suppresses reduction at high temperature, which leads to higher surface reactivity. It is reported that CeO_2 has the dominant ability to supply the active oxygen species which suppresses coke formation by oxidizing surface carbon on the catalyst active site [66].

The synthesis of supported catalysts is of greatest scientific and manufacturing importance. The essential requirements of obtaining well controlled uniformity and high-purity materials encouraged the development of wet chemical methods [79]. One of the important methods to prepare aluminates is combustion route [80]. The advantage of the solution combustion technique is the quasi-atomic dispersion of the component cations in liquid precursors, which facilitates synthesis of the crystallized powder with low particle size

and high purity at low temperatures [72]. Nevertheless, the ability to design and control size, structure, and dispersion of supported nanoparticles is still a great challenge.

In this work, nickel oxide based nanocomposites were prepared by template assisted wet-combustion synthesis method. This method includes wetting of the mesoporous network of a template (alumina) by a reactive solution containing the metal precursor and organic fuel, followed by the heat treatment until self-ignition of a combustion synthesis. The organic fuel can act as metal dispersing and complexing agent [81] and provide homogeneous distribution of metal precursors throughout the mesoporous network.

In order to choose the right fuel for mixed oxides composites of nickel, three additional systems were studied in this work: *Ni(NO$_3$)$_2$-glycine-ANF, Ni(NO$_3$)$_2$-urea-ANF and Ni(NO$_3$)$_2$-citric acid-ANF*. To obtain homogeneous and uniform nanocomposites, reactive aqueous solutions, containing stoichiometric amount of nickel (II) nitrate as a source of nickel and urea, glycine or citric acid as a fuel (eq. 3-5), were prepared and dropped onto the network of alumina nanofibers. The amounts of the precursors are represented in Table 3.

Table 3 *The composition of initial solution and the ratio of fuel to oxidizer.*

ANF, g	Ni(NO$_3$)$_2$*6H$_2$O,g	Urea, g	Glycine, g	Citric acid, g	H$_2$O, ml
1	2.84	0.32	0	0	5
1	2.84	0	0.81	0	5
1	2.84	0	0	1.04	5

$$9Ni(NO_3)_2 + 5CH_4N_2O = 3NiO + 8N_2 + 5CO_2 + 10H_2O \tag{3}$$

$$9Ni(NO_3)_2 + 10C_2H_5NO_2 = 9NiO + 14N_2 + 20CO_2 + 25H_2O \tag{4}$$

$$9Ni(NO_3)_2 + 5C_6H_8O_7 = 9NiO + 9N_2 + 30CO_2 + 20H_2O \tag{5}$$

X-ray diffraction analysis shows that the peaks of NiO along with low crystallinity peaks of NiAl$_2$O$_4$ are detected in nickel nitrate – glycine – ANF system Fig. 8(a). While using citric acid, peaks of nickel aluminate spinel with low crystallinity peaks of nickel oxide is obtained in XRD pattern Fig. 8(b). When urea is used as a fuel, only peak of NiO was evident in the XRD pattern Fig. 8(c). The different peaks obtained using different fuels can be explained on the basis of the more chelating nature of glycine and citric acid.

According to Nesaraj et al [62], glycine fuel serves two purposes in the combustion process for the preparation of nickel aluminate spinel: first, it complexes the metal cations (Ni

and Al), increasing their solubility and preventing selective precipitation of the salts as the water evaporates: and secondly, it serves as fuel for combustion. In case of urea as a fuel [62], accumulation of the hypergolic mixture of gases leads to the vigorous and spontaneous reaction. Urea imparts only energy to the reaction proved by Aghayan et al [63].

It should be noted that the peaks related to γ-Al_2O_3 phase are not detected in all cases. This can be caused by a destruction of the crystalline structure of γ-Al_2O_3, however, the maximum combustion temperature measured by pyrometric analyses, does not exceed 1100 ^oC (Table 4), which is lower than γ- to α- phase transformation [63]. To understand the reason of disappearance of the peaks of γ-Al_2O_3 more detailed investigation is needed.
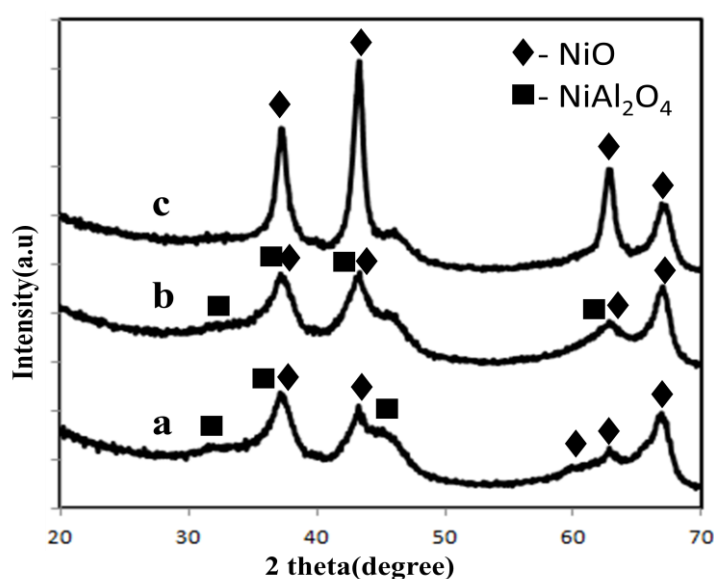

Figure 8 *XRD patterns of wet-combustion products of (a) nickel nitrate-glycine–ANF, (b) nickel nitrate –citric acid –ANF and (c) nickel nitrate – urea – ANF systems.*

Table 4 *Combustion flame temperature of nickel nitrate-fuel-ANF system measured by pyrometric method.*

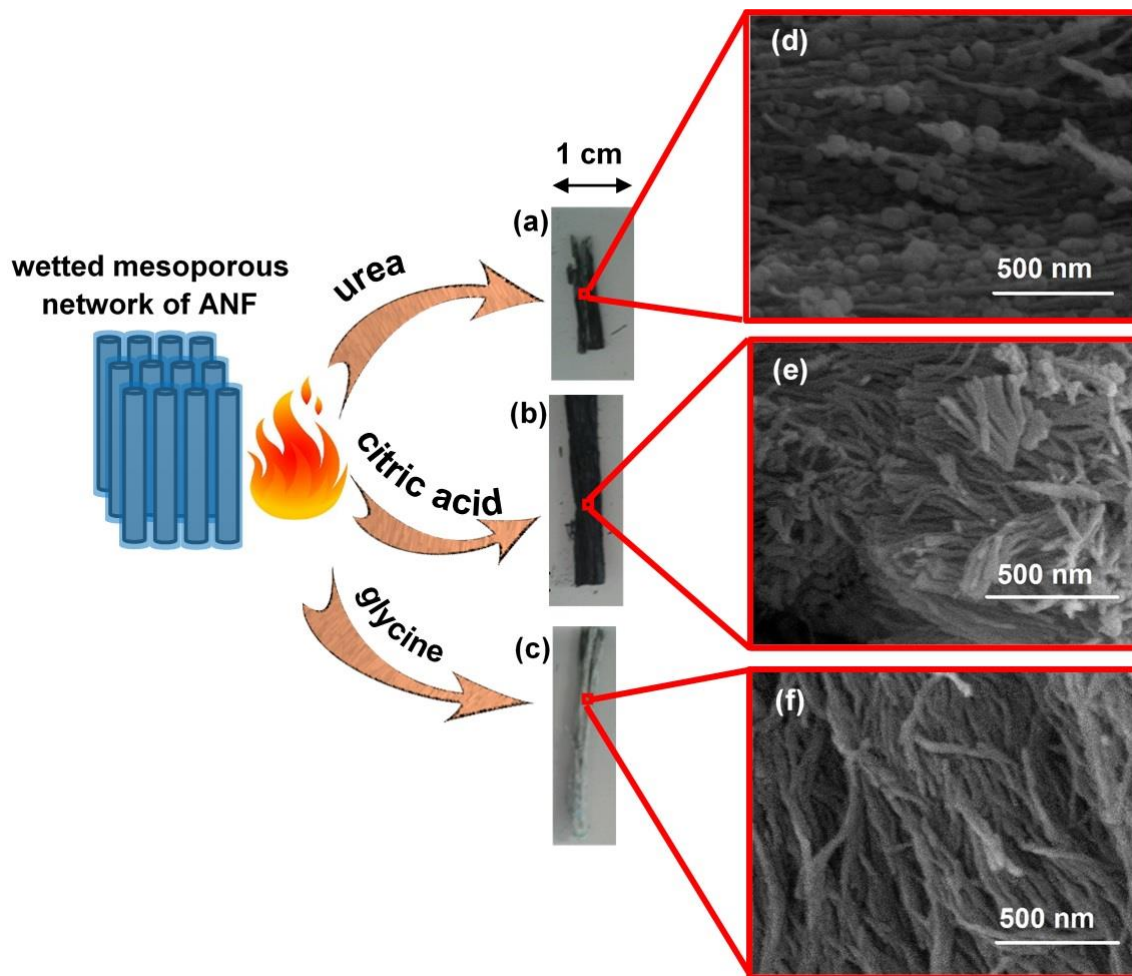| Fuel type	Flame temperature
Glycine	1005^oC
Citric acid	923^oC
Urea	1095^oC

Figure 9 *Schematic steps of the wet-combustion process of the wetted mesoporous network by the reactive solution containing different fuels, and, their corresponding SEM images: (d) nickel nitrate-urea-ANF, (e) nickel nitrate-citric acid-ANF, (f) nickel nitrate-glycine-ANF.*

The SEM images of the as-synthesized combustion products obtained from various fuel containing batches are demonstrated in Fig. 9(a-c). NiO with the fine particle size (<100 nm) forms when urea is used as a fuel. The particles are homogeneously deposited around the well aligned fibers. However, when glycine or citric acid were used as a fuel, only fibers in diameter <30 nm can be seen (Fig. 9(e, d)). It should be noted that in contrast to nickel nitrate-glycine-ANF system, the combustion of nickel nitrate-citric acid-ANF leads to the formation of broken fibers with length of 200-300 nm in Fig. 9(e).

Considering the obtained results, glycine is suggested as the best suited fuel for nickel nitrate – ANF system. Thus, for the further mixed oxide system only glycine was used as a fuel which was the main focus of the study.

In order to deposit nickel and cerium mixed oxides, and nickel and magnesium mixed oxides onto alumina nanofibers, stoichiometric amount (eq. (4, 6, 7)) of the nitrates of the mentioned oxides and glycine as a fuel are used to prepare the reactive solution with a proportion shown in Table 5.
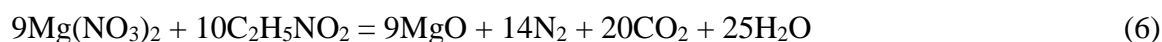
$$9Mg(NO_3)_2 + 10C_2H_5NO_2 = 9MgO + 14N_2 + 20CO_2 + 25H_2O \qquad (6)$$

$$18Ce(NO_3)_3 + 30C_2H_5NO_2 = 18CeO_2 + 42N_2 + 60CO_2 + 75H_2O \qquad (7)$$

Table 5 *The composition of initial solution.*

Ni(NO₃)₂*6H₂O,g	Mg(NO₃)₂*6H₂O,g	Ce(NO₃)₃*6H₂O,g	glycine, g	H₂O, ml
2.85	2.5	0	1.7	15
2.85	0	4.25	2.1	15
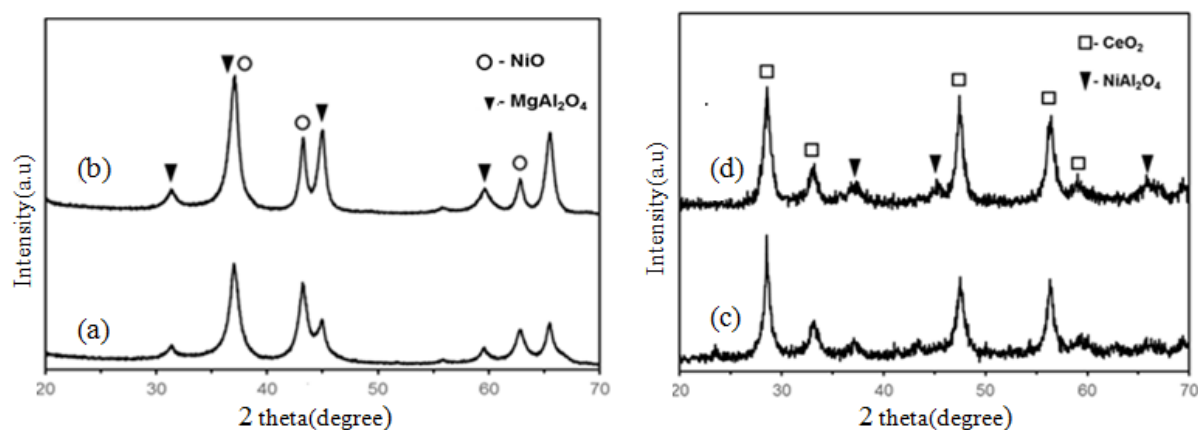
Figure 10 *XRD patterns of (a) combustion product, and (b) combustion product heat treated at 900°C of Ni(NO₃)₂-Mg(NO₃)₂-glycine-ANF system for 2hours, (c) combustion product, and (d) combustion product heat treated at 900°C of Ni(NO₃)₂-Ce(NO₃)₃-ANF system for 2 hours.*

The XRD pattern of Ni(NO₃)₂-Mg(NO₃)₂-glycine-ANF system is represented in Fig. 10(a-b). It should be noted that, NiAl₂O₄ and MgAl₂O₄ spinel-like phases are indistinguishable in XRD analysis. In general, the AB₂O₄ spinel structure consists of A^{2+} and B^{3+} ions where the cations can easily displace each other. Therefore, in the case of concurrency more likely MgAl₂O₄ spinel forms in Fig. 10(a) [54].

However, after heat treatment at 900^0C in Fig. 10(b), the intensity of the peak related to spinel increases. It is supposed that magnesium diffuses into alumina forming spinel which crystallizes during the heat treatment

The analysis signifies that heating of the sample at 900^oC leads to the expansion of the lattice. This expansive stress is created to the surface layer of the $MgAl_2O_4$ through dangling bonds. Hence ions on the surface of the nanoparticles of $MgAl_2O_4$ are not coordinated and have unpaired electrons. Al^{3+} and Mg^{2+} form the electric dipole on the boundary [68]. Due to heating, more oxygen atoms are added to the surface, these oxygen atoms combines with the dipole formed of Al^{3+} and Mg^{2+} which then forms incompletely coordinated aluminium-magnesium-oxygen atoms and thus spinel. So heating plays a huge role in increasing the crystal size of the spinel [68].

The XRD pattern of $Ni(NO_3)_2$-$Ce(NO_3)_3$-ANF system is presented in Fig. 10(c-d). The XRD patterns shows the existence of the distinct fluorite-type oxide structure of CeO_2 both in the combusted product in Fig. 10(c) and heat treated combusted product in Fig. 10(d). Besides CeO_2 peak, the intensity of $NiAl_2O_4$ spinel phase has very low crystallinity which is observed in both combusted and heat treated combusted product which may suggest that dispersion of nickel crystallite on CeO_2. Both the system can be better optimized using different content of the cerium. Koo et al [53] found that the peak intensity of NiO and $NiAl_2O_4$ is dependent on the Ce content. They noted that as cerium content increases, the intensity of NiO and $NiAl_2O_4$ peak decreases because ceria improves the dispersion of NiO and thus affects the solubility also.
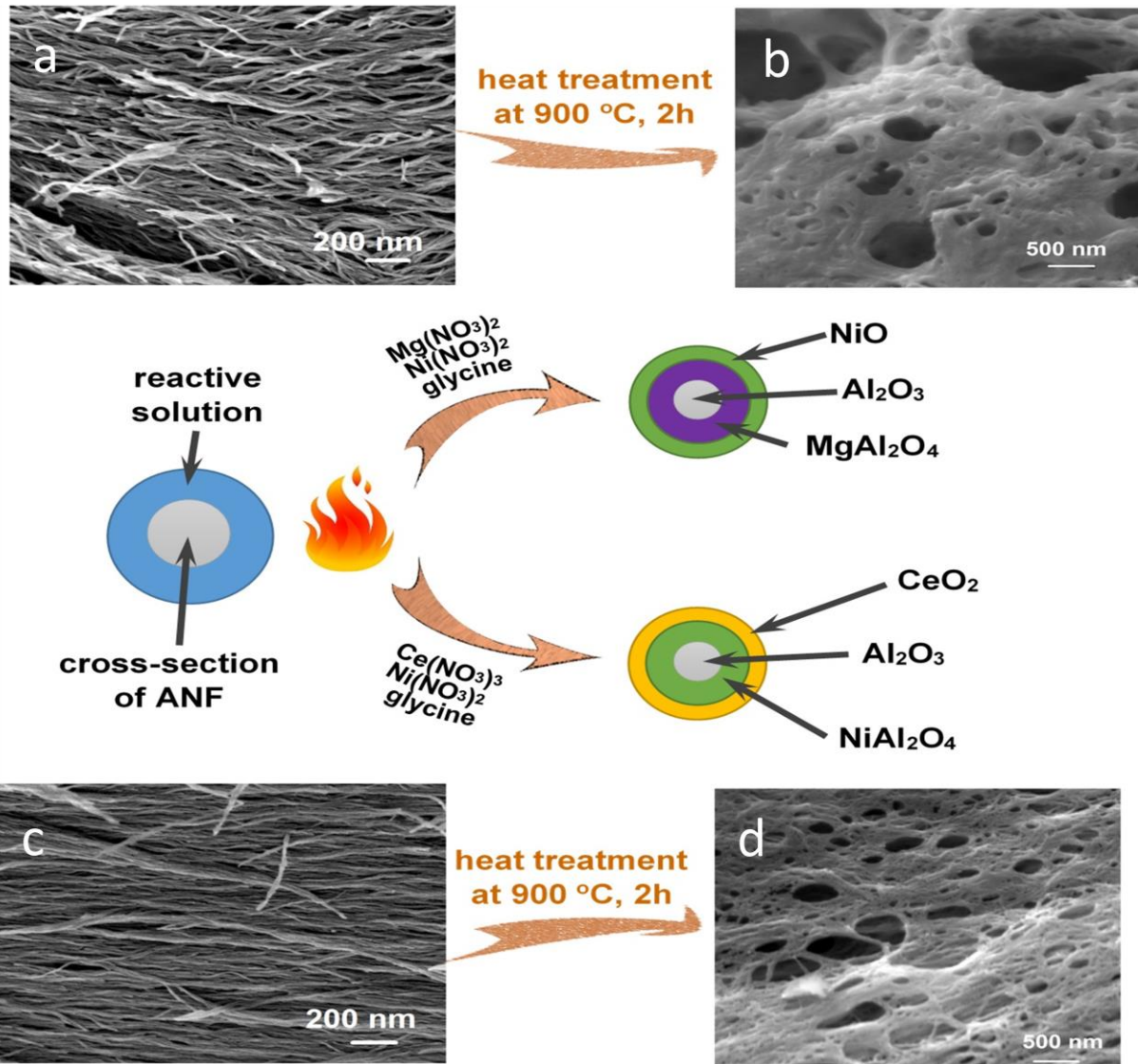
Figure 11 *Schematic view of the evolution of cross-section of a wetted single fiber during the wet-combustion process and corresponding SEM images: a) combustion product, and (b) combustion product heat treated at 900ºC of Ni(NO₃)₂-Mg(NO₃)₂-glycine-ANF system for 2hours, (c) combustion product, and (d) combustion product heat treated at 900ºC of Ni(NO₃)₂-Ce(NO₃)₃-ANF system for 2 hours.*

The combusted product of $Ni(NO_3)_2$-$Mg(NO_3)_2$-glycine ANF system consists of well aligned regular shape nanofibers as illustrated in Fig. 11(a) and the particles are homogeneously deposited on fibers. The heat treated combusted product obtained from $Ni(NO_3)_2$-$Mg(NO_3)_2$-glycine ANF system reveals that system is porous in SEM micrograph Fig. 11(b). The heat treated combustion product obtained from $Ni(NO_3)_2$-$Ce(NO_3)_3$-ANF

system in Fig. 11(d), consists of the alignment of the nanofibers in the similar fashion as it was observed in $Ni(NO_3)_2$-$Mg(NO_3)_2$-glycine ANF system.

With the heat treatment of the combusted products in both the system of $Ni(NO_3)_2$-$Mg(NO_3)_2$-ANF and $Ni(NO_3)_2$-$Ce(NO_3)_3$-ANF system, it is believed that nickel surface area and nickel dispersion is affected due to readily formation of MgO and CeO_2 as explained in the cross section diagram of the both $Ni(NO_3)_2$-$Mg(NO_3)_2$-ANF and $Ni(NO_3)_2$-$Ce(NO_3)_3$-ANF system in Fig. 11 . These oxides obtained after combustion affects the textural properties of alumina. CeO_2 readily supplies the active oxygen species which can readily eliminate the formation of the coke in the catalyst reactions [66]. However, detailed catalytic studies are needed to prove the analysis.

4.3   Iron oxide based nanocomposites

Hematite (α-Fe_2O_3), the most thermodynamically stable phase of iron trioxide and recent efforts have been directed towards the fabrication of nanoscale α-Fe_2O_3 to enhance its performance in currently existing applications of catalysts, pigments, gas sensors, optical devices, and water purification. The nanostructures of iron oxides with different dimensionalities such as nanoparticles, nanorods, nanowires, nanotubes, nanorings, nanobelts, nanocubes, as well as hollow and porous nanostructures have been successfully used in various fields, including energy conversion and storage technologies [56].

A Pt gamma -alumina catalyst promoted with iron oxide deposited on a ceramic monolith was recently reported to be highly active, selective, and stable for the CO oxidation reaction in the presence of excess H_2 at temperatures compatible with the PEM fuel cell [82]. However, the stand alone properties of hematite (α-Fe_2O_3), to exhibit magnetic properties have attracted much attention of the researchers.

Among synthesis methods of hematite to be used as a magnetic material, various efforts were made by researchers. For example, spherical carbon nanoparticles or carbon nanotubes have been used as templates for the synthesis of hollow spheres and nanotubes of hematite [83]. Recently, iron-containing metal−organic frameworks and ferritin proteins were proposed as templates to prepare clusters of hematite nanoparticles through controlled pyrolysis [84]. Work reported by Mukasyan et al reported a new strategy for preparation of ultrasmall (below 5 nm) superparamagnetic hematite nanoparticles with remarkably high magnetization. They successfully integrated a combustion approach with template-assisted synthesis [56].

In this work, iron oxide based nanocomposites are prepared using iron nitrate and glycine and urea as a fuel with different fuel-to-oxidizer ratios (Table 6) by wet combustion method

.

Table 6 Preparation of solutions with different oxidizer fuel ratio (φ)

N of sol	ANF, g	Fe(NO₃)₃*9H₂O,g	Urea, g	Glycine,g	H₂O, ml	Φ
1	0.5	5	0.93	0	5	0.5
2	0.5	5	1.86	0	5	1.0
3	0.5	5	2.79	0	5	1.5
4	0.5	5	0	0.77	5	0.5
5	0.5	5	0	1.55	5	1.0
6	0.5	5	0	2.32	5	1.5

In the above, φ=1 means that the initial mixture does not require atmospheric oxygen for complete oxidation of fuel, while φ > 1 implies fuel rich and φ < 1 implies fuel lean conditions. The following (eq 8 and 9) were used.

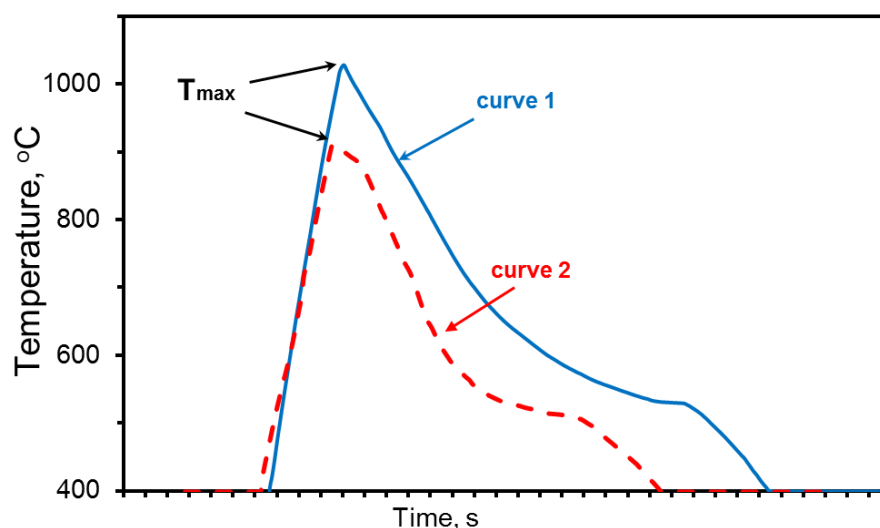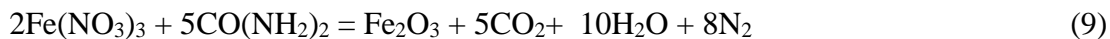$$3Fe(NO_3)_3 + 5C_2H_5NO_2 = 3/2Fe_2O_3 + 10CO_2 + 12.5H_2O + 7N_2 \tag{8}$$

$$2Fe(NO_3)_3 + 5CO(NH_2)_2 = Fe_2O_3 + 5CO_2 + 10H_2O + 8N_2 \tag{9}$$

Figure 12 *Combustion flame temperature of Fe(NO₃)₃– glycine – ANF system (curve1), and Fe(NO₃)₃– urea – ANF system (curve 2).*

The typical time-temperature profiles for combustion synthesis process of iron nitrate-glycine alumina nanofibers and iron nitrate-urea-alumina nanofibers systems with oxidizer to fuel ratio, $\varphi=1$ is shown in Fig. 12 (curve1 and 2 respectively). Series of changes in the sample which is followed by sudden rise of temperature rise to a maximum (T_{max}) value. When the temperature reaches to maximum (T_{max}) value, rapid reaction takes place. It can be seen that T_{max} varies of the fuel type. The maximum temperatures observed were ~1030 °C in the glycine system ($\phi_{gly}= 1$) and ~900 °C in urea system ($\phi_{ur}=1$). It was noted that increase of the media volume during the combustion of iron nitrate - glycine –ANF system takes place. While the volume of the final solid product is not different from the initial wetted sample when urea was used as a fuel.
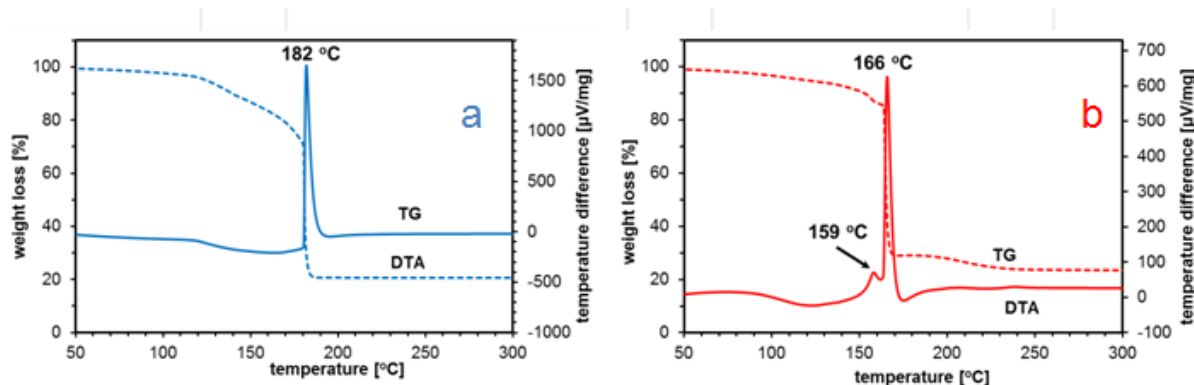

Figure 13 *(a) DTA/TG curve of iron nitrate-glycine-ANF and (b) iron nitrate-urea-ANF. Curve1 represents TGA and curve 2 represents DTA in both the cases.*

In order to understand the kinetics of combustion impregnation process TGA–DTA was performed at heating $10°C/min$ from ambient temperature upward to $300°C$ under air atmosphere. In Fig. 13(a) TG curve indicated that the mass of the dried gel starts decreasing evidently/distinguishably from $120°C$ accompanied by an endothermic effect in the DTA curve in iron nitrate-glycine-ANF system. It is reasonably supposed to be the dehydration of the intercalated water in the formed complex of dried gel. The mass loss becomes more intensive from $170°C$ to $205°C$ accompanied with the sharp exothermic reaction, which is characterized as the typical combustion process. In the end the gel losses 80% of its initial mass.

According to Varma et al [69] the $Fe(NO_3)_3.3H_2O$ decomposition occurs according to the following eq 10:

$$Fe(NO_3)_3.3H_2O \rightarrow Fe(OH)_2NO_3 \rightarrow Fe(OH)_3 \rightarrow Fe_2O_3. \tag{10}$$
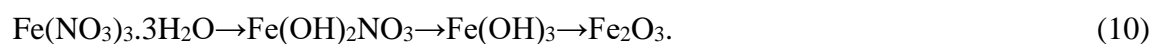
Thus, during this decomposition HNO_3 forms, this immediately (either directly or with preliminary oxygen formation) reacts with glycine. Combustion in the glycine-nitrate system starts with oxidizer decomposition which is followed by decomposition of glycine [70] proved by Yablokov et al which starts from the temperature range of 212-240°C.

The reaction proceeds differently when using urea as the fuel Fig. 13(b) in iron nitrate-urea-ANF system. The process starts with the decomposition of urea which starts at 152°C studied by Schaber et al [71]. Before 155°C, a weight loss of 11 % was caused by evaporation of water and from 155°C to 164, a weight loss of 4%, which announce the start of the decomposition of urea [71]. The decomposition of urea leads to biuret and NH_3 release. From 155°C to 168°C, a weight loss of 55% together with an exothermic peak at 166 °C is attributed to the combustion process. It should be noted that the combustion takes place at relatively lower temperature compared with glycine system.
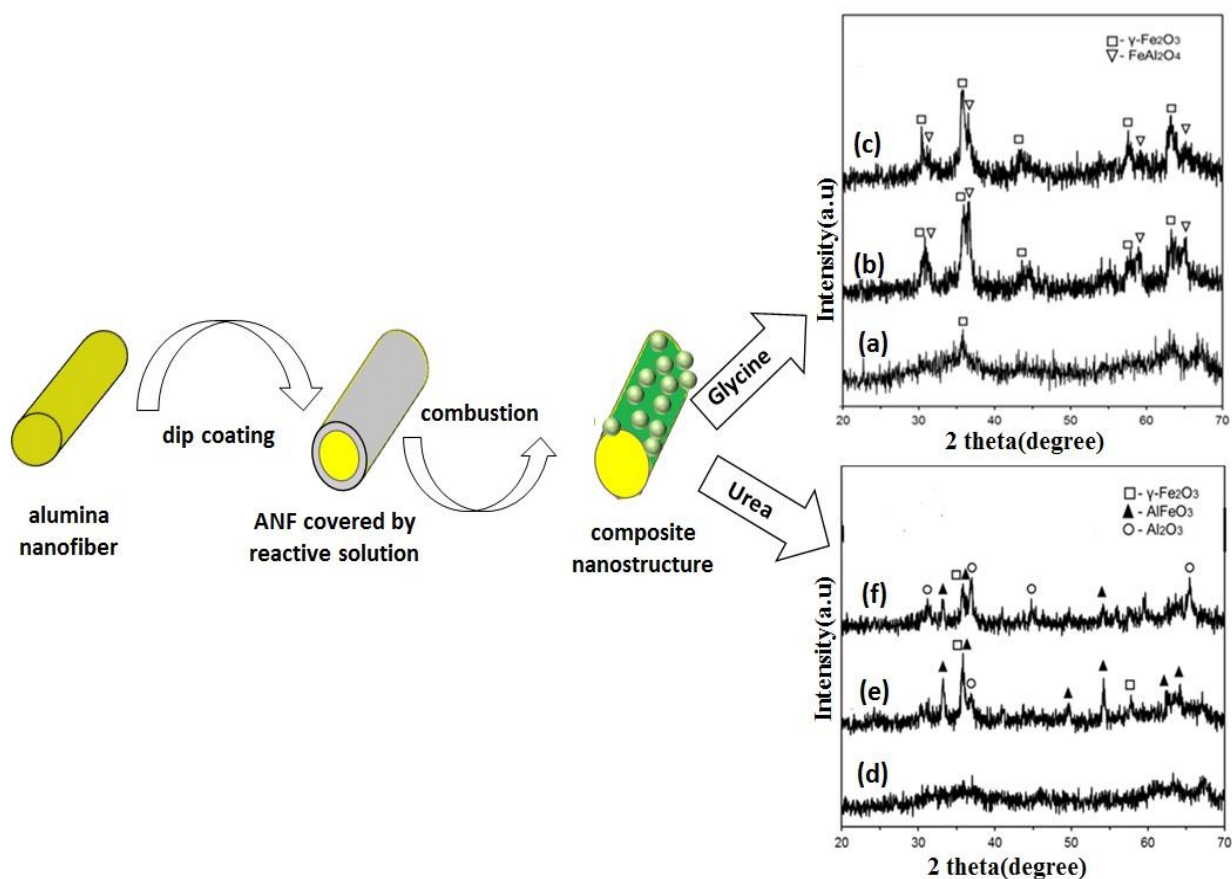

Figure 14 *Schematic view of the evolution of cross-section of a wetted single fiber during the wet-combustion process towards the formation of composite and corresponding XRD pattern of iron nitrate-glycine-ANF with oxidizer to fuel ratio (ϕ) (a) 0.5, (b) 1, and (c) 1.5 and pattern of iron nitrate-urea-ANF with oxidizer to fuel ratio (ϕ) (d) 0.5, (e) 1, and (f) 1.5.*

XRD data on phase composition of the final products obtained by heterogeneous combustion synthesis from systems with different oxidizer to fuel φ, are presented in Fig. 14(a, b and c). An amorphous product forms with a small broad peak with low oxidizer to fuel ratio, φ=0.5 in Fig 14(a) of iron nitrate-glycine-ANF, whereas a mixture of γ-Fe_2O_3 and $FeAl_2O_4$ formed for a system with oxidizer to fuel ratio, φ =1 in Fig. 14(b). The intensity of peaks of $FeAl_2O_4$ decreases with increasing the glycine amount with oxidizer to fuel ratio, φ=1.5 in Fig. 14(c). It is supposed that during combustion process reduced oxide of iron (Fe_3O_4) forms which reacts with alumina nanofibers leading to the formation of $FeAl_2O_4$. The possibility of formation of Fe_3O_4 during combustion was proved by thermodynamic calculation done by Mukasyan et al. [72]. Xiang et al. [73] reported that reaction between Fe_3O_4 and Al_2O_3 takes place over 600°C under reducing atmosphere leading to the formation of $FeAl_2O_4$. It should be noted that in the fuel – rich system, the ratio of the obtained $FeAl_2O_4$/Fe_2O_3 decreases with increasing the glycine amount as the oxidant fuel ratio is changed from 1 to 1.5. This is caused by the decrease of the combustion temperature by increasing the amount of fuel. [72]. The low temperature drastically influences the interaction of Fe_3O_4 with alumina. Thus, glycine appears to be not only a source of energy, but also a reducing agent, enabling to produce nanocomposite in a single step.

Using small amount of urea with oxidizer to fuel ratio, φ=0.5 in Fig. 14(d), amorphous mass is formed in iron nitrate-urea-ANF system. Increasing the amount of urea, the dominant phase is identified as rhombohedral $FeAlO_3$. Small amount of α-Al_2O_3 and γ-Fe_2O_3 is also formed with oxidizer to fuel ratio, φ=1 in Fig. 14(e). The direct interaction between iron ions and alumina is possible, however, due to the high temperature developed during the combustion process $FeAlO_3$ phase forms. Although, Hamasake et al. [74] reported that alumina and hematite coexisted under below 1300 °C. Recently few researchers could synthesize rhombohedral $FeAlO_3$ at lower temperatures (below 600°C) proved by Cotica et al [75] by sol-gel method. Increasing the amount of urea, iron ions become more isolated by urea preventing the formation of $FeAlO_3$ phase and hence proves the obtained XRD result of increase of the crystallinity of α-Al_2O_3 with oxidizer to fuel ratio, φ=1.5 in Fig. 14(f). Only Fe (III) oxides were obtained in when urea was used, while the reduced Fe (II) oxide (in spinel form) was obtained when glycine is used.

Fig. 15(a-b) represents SEM micrographs of as-synthesized-deposited product of iron nitrate – glycine – ANF system. At the fuel-lean glycine system in Fig. 15(a), an agglomeration of well aligned fibers takes place. However, at stoichiometric amount of

glycine the particles with less than 100 nm were formed and the fibers became more discontinuous shown in Fig. 15(b). The increase of particle size is understandable due to increase in oxidizer to fuel ratio. It is supposed that the particles are composed of Fe_2O_3. Thus, nucleation occurs by the formation of small embryos of Fe_2O_3 inside the small volume of organometallic network structure. This network structures form when an appropriate amount of chelating agent (i.e. glycine and glycine contaminations) coordinates iron and surface aluminium ions.
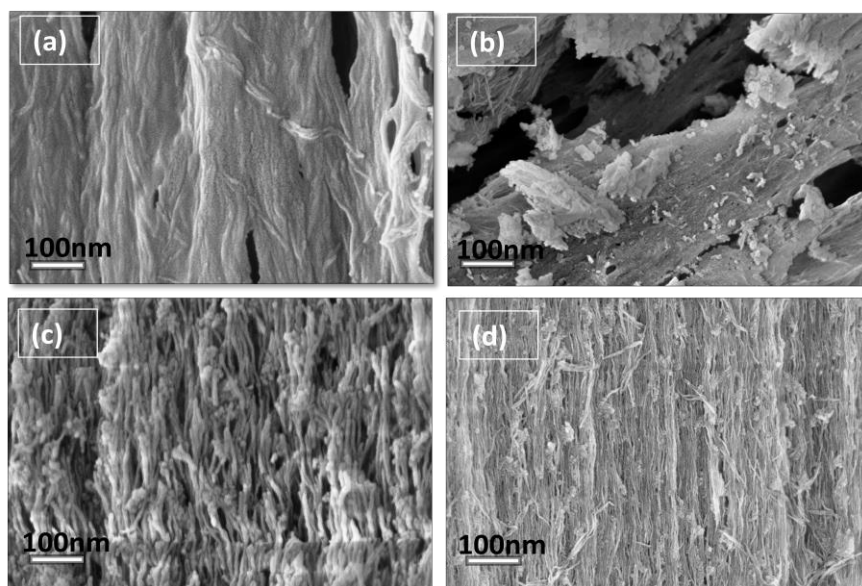

Figure 15 *SEM micrographs of iron nitrate-glycine-ANF with oxidizer to fuel ratio (ϕ) (a) 0.5, (b) 1 and of iron nitrate-urea-ANF with oxidizer to fuel ratio (ϕ) (c) 0.5, (d) 1.*

As shown in the Fig. 15(c-d), the SEM micrographs of as-synthesized-deposited product of iron nitrate – urea – ANF system, an agglomeration of well aligned fibers takes place in Fig. 15(c). The fibers look "broken" periodically, when oxidizer to fuel ratio is φ_{ur}=0.5 in Fig. 15(c). The as-prepared product, when oxidizer to fuel ratio, φ_{ur}=1, are continuous in structure in Fig. 15(d). Between the fibers, agglomerations of small particles of Fe_2O_3 were believed to exist.

Fig. 16 represents the magnetic characterization at room-temperature of both products of Fe_2O_3-Al_2O_3 using glycine and urea. The magnetization as a function of applied magnetic field clearly shows hysteretic behavior, revealing the existence of ferro- and/or ferrimagnetic order in the both the systems. The Fe_2O_3-Al_2O_3-glycine system exhibits a saturation magnetization (Ms) and remanence (Mr) of 40 emu/g and 14 emu/g respectively. In the case of the Fe_2O_3- Al_2O_3-urea system, Ms and Mr amount to 28 emu/g and 8 emu/g respectively
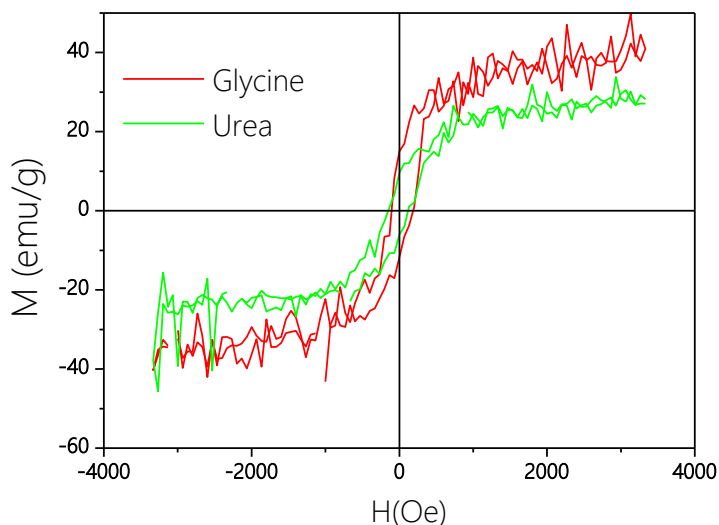
Figure 16 *Magnetization vs. applied field curves at room-temperature corresponding to the products synthesized using Glycine and Urea.*

Maghemite (γ-Fe_2O_3) is ferrimagnetic at room temperature with a saturation magnetization of 74 emu/g. Given the saturation magnetization (Ms) value of the pure compound, one can estimate the compositional ratio of phases more accurately than the XRD data. It is inferred that in the glycine and urea sample the weight fraction of maghemite reaches 54% and 38% respectively.

It is worth noting that the glycine system contains $FeAl_2O_4$, which is antiferromagnetic and known to exhibit weak ferromagnetism due to frustration effects [76]. However, this weak contribution to saturation magnetization (Ms) can be disregarded as it is expected to be below 1 emu/g [77].

5. CONCLUSIONS

In this work, mesoporous substrates consisting out of composite nanofibers were prepared by wet combustion synthesis without further calcination and it was demonstrated that the template-assisted wet-combustion synthesis approach is a flexible technique to deposit metal oxide onto alumina nanofibers using one-step process for production of network with tailored phase composition and morphology.

Thus nanocomposites with different composition and morphology were obtained by varying oxidizer-fuel ratio and the fuel which act as a source of energy.

The two systems were rigorously studied and following remarks can be pointed out:

- **Nickel oxide based nanocomposites:** Heteronanostructures of the metal oxides core-shell nanofibers $NiO-NiAl_2O_4-Al_2O_3$ were deposited onto the network of nanofibers. It was observed that NiO along with traces of $NiAl_2O_4$ are detected in nickel nitrate – glycine – ANF system. When urea is used as a fuel, only peak of NiO is detected. While using citric acid, mainly nickel aluminate spinel with traces of nickel oxide was obtained. Hence proving that composition of the product can be controlled by different fuels (glycine, urea, and citric acid). Considering the obtained results from SEM of $Ni(NO_3)_2$-ANF system composites, glycine is suited as the best fuel. To further extend the research, mixed composition of $Ni(NO_3)_2$-$Mg(NO_3)_2$-ANF and $Ni(NO_3)_2$-$Ce(NO_3)_3$-ANF system were used for the catalytic applications. Glycine is opted as the fuel based on the results of SEM micrographs of $Ni(NO_3)_2$-ANF system. The mixed oxides obtained after the combustion of $Mg(NO_3)_2$-ANF and $Ni(NO_3)_2$-$Ce(NO_3)_3$-ANF system can enhance the dispersivity of nickel.

$Ni(NO_3)_2$-$Ce(NO_3)_3$ and $Ni(NO_3)_2$-$Mg(NO_3)_2$ ANF system revealed that mixed oxides CeO_2-$NiAl_2O_4$ and NiO-$MgAl_2O_4$ were deposited on alumina nanofibers respectively. The deposited heteronanostructures of the metal oxides core-shell nanofibers had a significance influence the combustion pathway of ANF-fuel system. However more profound studies can be done by adding different proportions of ceria and magnesium which can affect nickel oxide solubility and dispersion.

- **Iron oxide based nanocomposites**: Highly aligned alumina nanofibers were functionalized by iron oxide using glycine and urea as a fuel. The XRD results shows that only Fe (III) oxides were obtained in when urea was used, while the reduced Fe (II) oxide (in spinel form) was obtained when glycine is used by varying oxidizer to fuel ratio. Glycine

appears to be not only a source of energy, but also a reducing agent, enabling to produce nanocomposite in a single step.

The magnetic properties revealed that Fe_2O_3-Al_2O_3-glycine system exhibits a saturation magnetization and remanence of 40 emu/g and 14 emu/g whereas in Fe_2O_3- Al_2O_3 urea system, saturation magnetization and remanence amounts to be 28 emu/g and 8 emu/g respectively. At last it is inferred that in glycine and urea sample, the weight fraction of maghemite reaches 54% and 38% respectively.

To conclude, solution combustion synthesis is the best method to fabricate mesoporous fibrous structures consisting of the networks of nanocomposite nanofibers.

6.   RÈSUMÈ

The alumina nanocomposite formed from the nanofibers is regarded as the most important ceramic engineering material not only because of the well-known properties of corrosion-erosion-resistant material but also possibilities of improving these nanocomposites due to its relative cost than other materials. Today most of the alumina composites find its application in fabrication of high temperature refractory materials and many more.

In this study new type of nanocomposites using ANF as the support were created. To prepare these composites one-step procedure using novel approach of the template-assisted wet-combustion synthesis, which combines combustion synthesis and dip coat methods were used which was developed by our group to functionalize nano-objects. Various nanocomposites were synthesized by our group utilizing this method.

The nanocomposites of $NiO-Al_2O_3$, $MgAl_2O_4-NiO-Al_2O_3$, $CeO_2-NiAl_2O_4-Al_2O_3$ and $Fe_2O_3-Al_2O_3$ are characterized by XRD, SEM-EDS, DTA/TG and magnetic techniques.

At the very first time, $NiO-NiAl_2O_4$, $NiAl_2O_4-Al_2O_3$ and $NiO-Al_2O_3$ composites were fabricated by wet-combustion method revealed by XRD studies using different fuels. The SEM micrographs of $Ni(NO_3)_2$-ANF fuel system revealed that glycine is the best suited fuel because when compared with other fuels (urea and citric acid), the particles are more homogenously deposited onto the network of well aligned fibers. Based on these results, glycine is opted for the mixed oxides of $Mg(NO_3)_2$-ANF and $Ni(NO_3)_2-Ce(NO_3)_3$-ANF system to carry out the further research.

The mixed oxides of $CeO_2-NiAl_2O_4$ and $NiO-MgAl_2O_4$ were deposited on alumina nanofibers respectively. The deposited heteronanostructure of the metal oxides core-shell nanofibers had influence on the dispersivity of nickel.

In $Fe_2O_3-Al_2O_3$ composites synthesized using different fuels, XRD studies revealed that Fe (III) oxides were obtained in when urea was used, while the reduced Fe (II) oxide (in spinel form) was obtained when glycine is used. The thermal studies on the composites shows that maximum temperatures observed were ~1030 ℃ in the glycine system ($\phi_{gly}= 1$) and ~900 ℃ in urea system ($\phi_{ur}=1$). The magnetic properties revealed that $Fe_2O_3-Al_2O_3$-glycine exhibits a saturation magnetization and remanence of 40 emu/g and 14 emu/g whereas in $Fe_2O_3-Al_2O_3$-urea, saturation magnetization and remanence amounts to be 28 emu/g and 8 emu/g respectively. Saturation magnetization was less in the case of urea because weight fraction of maghemite reaches only 38% but in case of glycine it reaches 54%.

To summarize, solution combustion synthesis is the best method to fabricate nanocomposites. The advantages of process are that wet-combustion method uniquely combines the merits of a sol-gel method (e.g., homogeneous distribution of components, low temperature) and a solution combustion process (e.g., high temperature, fast heating rate and short duration).

7.   RESÜMEE

Hiljuti väljatöötatud ühedimensionaalsed γ-alumiiniumoksiidist (Al_2O_3) nanokiud, läbimõõduga 7±2 nm, on funktsionaliseeritud uudse märg-põlemise meetodiga. Funktsionaliseerimise eesmärgiks on laiendada nende kasutusvaldkonda erinevates funktsionaalsetes komposiitmaterjalides. Märg-põlemise meetod ühendab endas sool-geel meetodi (homogeenne komponentide jagunemine ja madal temperatuur), sisse-kastmis pindamise (lihtsus, mikrostruktuuri kontroll ja kuluefektiivsus) ja põlemise meetodi (kõrge temperatuur, kiire kuumutus ja lühike kestvus) eeliseid. Märg-põlemise süntees on üheetapiline lähenemine võimaldades kuluefektiivselt sünteesida mesopoorseid komposiite, millel on eesmärgipäraselt disainitud faasiline kompositsioon ja morfoloogia. Väljatöötatud meetodi raames kaetakse nanokiud lähtematerjalidest lisanditega, mis on segatud orgaaniliste kütustega. Sellele järgneb lähtematerjalide ja kütuse lagunemine/oksüdeerumine, mille tulemusel toimub nanokiudude pindamine uue faasiga või terve nanokiu faasi muutumine. Protsessis tulemusena saab valmistada 1D nanostruktuuridega komposiitmaterjale, millele jääb alles nende originaalne morfoloogia ning soovitud keemiline kompositsioon.

Antud töö eesmärgiks oli keraamiliste nano-komposiitmaterjalide NiO-Al_2O_3, $MgAl_2O_4$-NiO-Al_2O_3, CeO_2-$NiAl_2O_4$-Al_2O_3 ja Fe_2O_3-Al_2O_3 väljatöötamine. Eesmärgi saavutamiseks läheneti probleemile mitmest suunast, hõlmates sool-geel tehnoloogiat, materjalide töötlust kõrgetel temperatuuridel, täppis-karakteriseerimise meetodeid (XRD, SEM-EDS, DTA/TG ja magnetitehnoloogia) ja nano-osiste füüsikaliste omaduste selgitamist.

Alumiiniumoksiid nanokiude funktsionaliseeriti erinevate metallioksiididega (nt. NiO, MgO_2, CeO_2 ning Fe_2O_3) rakendades uut väljatöötatud märg-põlemise sünteesi olles alternatiiv sool-geel süntees pindamisemeetoditele. Esmakordselt on valmistatud mesopoorsed nanostruktuurid, mis omavad struktuure läbimõõduga alla 50 nm ilma, et oleks vaja järelkaltsineerimist.

Märg-põlemise meetodi kasutamise eeliseks nano-komposiitmaterjalide ja funktsionaalsete katete väljatöötamisel on paindlikkus ja võimalus valmistada samast lähteainest väga erinevaid objekte: pinnakatteid, komposiite, fiibreid, ja pulbreid.

8.   REFERENCES.

[1] Planning and Research Office, N., A Vision of Materials Science in the Year 2020, 2007.

[2] Y. Zuo, Y. Zhao, X. Li, N. Li, X. Bai, S. Qiu, W. Yu Synthesis of alumina nanowires and nanorods by anodic oxidation method, Mater. Lett., 60(24),(2006):2937.

[3] Ahmed, W., et al. "Effect of textural properties of alumina support on the catalytic performance of Ni/Al 2 O 3 catalysts for hydrogen production via methane decomposition." Journal of Natural Gas Science and Engineering 25 (2015): 359-366.

[4] Peintinger, Michael F., Michael J. Kratz, and Thomas Bredow. "Quantum-chemical study of stable, meta-stable and high-pressure alumina polymorphs and aluminum hydroxides." Journal of Materials Chemistry A 2.32 (2014): 13143-13158.

[5] Cai, Shu-Hui, et al. "Atomic scale mechanism of the transformation of γ-alumina to θ-alumina." Physical review letters 89.23 (2002): 235501.

[6] Jiang, Zhou Qing, et al. "Effects of Urea/Al3+ Ratios and Hydrothermal Treated Time on the Formation of Self-Assembled Boehmite Hollow Sphere." Ferroelectrics 471.1 (2014): 128-138.

[7] A.C. Vieira Coelho, G.A. Rocha, P. Souza Santos, H. Souza Santos, P.K. Kiyohara, Specific surface area and structures of aluminas from fibrillar pseudoboehmite,Revista Matéria, 13 (2) (2008), pp. 329–341.

[8] Petr Ptáček (2014). Processes during Thermal Treatment, Strontium Aluminate - Cement Fundamentals, Manufacturing, Hydration, Setting Behaviour and Applications, Associate Prof. Petr Ptáček (Ed.), InTech, DOI: 10.5772/58609.

[9] S. K. Dhoke, T. J. Mangal Sinha, and A. S. Khanna, "Effect of nano-Al2O3 particles on the corrosion behavior of alkyd based waterborne coatings," Journal of Coatings Technology Research, vol. 6, no. 3, pp. 353–368, 2009.

[10] J. Adánez, L.F. de Diego, F. García-Labiano, P. Gayán, A. Abad, J.M. Palacios, , " Selection of oxygen carriers for chemical-looping combustion," Energy Fuels, 18 (2) (2004), pp. 371–377

[11] T. Mattisson, A. Järdnäs, A. Lyngfelt , " Reactivity of some metal oxides supported on alumina with alternating methane and oxygen – application for chemical-looping combustion," Energy Fuels, 17 (2003), pp. 643–651.

[12] Yung, Matthew M., Whitney S. Jablonski, and Kimberly A. Magrini-Bair. "Review of catalytic conditioning of biomass-derived syngas." Energy & Fuels 23.4 (2009): 1874-1887.

[13] Ganley, J. C., et al. "Porous anodic alumina optimized as a catalyst support for microreactors." Journal of Catalysis 227.1 (2004): 26-32.

[14] Attaluri, Anil Chandra, et al. "Evaluation of nano-porous alumina membranes for hemodialysis application." ASAIO journal 55.3 (2009): 217-223.

[15] C. G. Chateld, J. N. Lindstrom, M. E. K. Sjostrand and I. K. M. Collin, CVD of Al2O3 layers on cutting inserts, 1996, US Patent 5,543,176.

[16] G. Paglia, C. E. Buckley, A. L. Rohl, R. D. Hart, K. Winter, A. J. Studer, B. A. Hunter and J. V. Hanna, Chem. Mater.2004, 16, 220–236.

[17] M. Minnermann, B. Neumann, V. Zielasek and M. Baumer, Catal. Sci. Technol., 2013, 3, 3256–3267.

[18] S.A. Bagshaw, T.J. Pinnavaia, Mesoporous Alumina Molecular Sieves, Angew. Chem. (Intern.Ed.English) (1996), 35 (10): 1102-1105

[19] G. Lu, P. Chang, Z. Fan, Quasi-one-dimensional metal oxide materials—Synthesis, properties and applications Mater. Sci. Engineer. R: Reports, 52(1-3), (2006):49-91.

[20] oh, G.L., K.Y. Liew, and W.A.K. Mahmood, Synthesis and characterization of sol–gel alumina nanofibers. Journal of Sol-Gel Science and Technology, 2007. 44(3): p. 177-186.

[21] R.L. Price, L.G. Gutwein, L. Kaledin, F. Tepper, T.J. Webster, Osteoblast function on nanophase alumina materials: influence of chemistry, phase, and topography, J. Biomed Mater Res, 67 (4) (2003), pp. 1284–1293.

[22] R.L. Price, K.M. Haberstroh, T.J. Webster, Enhanced functions of osteoblasts on nanostructured surfaces of carbon and alumina, Med Biol Eng Comput, 41 (2003), pp. 372–375.

[23] O. Boni, S. Berger, Dielectric properties of KDP filled porous alumina nanocomposite thin films, J Nanosci Nanotechnol, 4 (2001), pp. 433–439.

[24] Webster, Thomas J., Elaine L. Hellenmeyer, and Rachel L. Price. "Increased osteoblast functions on theta+ delta nanofiber alumina." Biomaterials 26.9 (2005): 953-960.

[25] Ke, X.B., et al., High-Performance Ceramic Membranes with a Separation Layer of Metal Oxide Nanofibers. Advanced Materials, 2007. 19(6): p. 785-790.

[26] Shen, S.-C., Ng, W. K, Zhong, Z.-Y., Dong, Y.-C., Chia, L., Tan, R. B. H., Solid-Based Hydrothermal Synthesis and Characterization of Alumina Nanofibers with Controllable Aspect Ratios, J. Am. Ceram. Soc., 2009, 92, 131.

[27] Guo, B., Yim, H., Luo, Z.P., Formation of alumina nanofibers in carbon-containing coflow laminar diffusion flames, J. Aerosol Sci., 2009, 40, 379.

[28] Yang, Q., Deng, Y., Hu, W., Synthesis of alumina nanofibers by a mercury-mediated method, Ceram. Intern., 2009, 35, 531.

[29] Noordin, M.R., Liew, K.Y., Synthesis of Alumina Nanofibers and Composites, Nanofibers, Intech, 2010.

[30] Azad, A. M., Fabrication of transparent alumina (Al2O3) nanofibers by electrospinning, Mater. Sci. Eng. A, 2006, 435-436, 468. ; Panda, P. K., Ramakrisna, S., Eletrospinning of alumina nanofibers using different precursors, J. Mater. Sci., 2007, 42, 2189.

[31] E. Liu, Synthesis of one-dimensional nanocomposites based on alumina nanofibers and their catalytic applications PhD Thesis, Queensland University of Technology (2011).

[32] Zhu, Huai Yong, James D. Riches, and John C. Barry. "γ-alumina nanofibers prepared from aluminum hydrate with poly (ethylene oxide) surfactant." Chemistry of Materials 14.5 (2002): 2086-2093.

[33] Paola Palmero, Frank Kern, Frank Sommer, Mariangela Lombardi, Rainer Gadow, Laura Montanaro, Issues in nanocomposite ceramic engineering: focus on processing and properties of alumina-based composites, J Appl Biomater Funct Mater 2014; 12 (3): 113-128.

[34] T.N Tiegs, and P.F.Becher, "Alumina-SiC whisker composites", Dept of energy conference report CONF-8510103-5(1985).

[35] Voltsihhin, Nikolai, et al. "Low temperature, spark plasma sintering behavior of zirconia added by a novel type of alumina nanofibers." Ceramics International 40.5 (2014): 7235-7244.

[36] Aruna, S. T., and K. S. Rajam. "Mixture of fuels approach for the solution combustion synthesis of Al 2 O 3–ZrO 2 nanocomposite." Materials research bulletin 39.2 (2004): 157-167.

[37] A. P Glaushkin, K.YA. Salnikov, "High-Thermostability Aluminochromosilicte Fiber", Rarefactories, 16[5] 318(1975).

[38] Aghayan, A., et al., A novel approach to electroconductive ceramics filled by graphene covered nanofibers. Materials & Design, 2016. 90: p. 291-298.

[39] Cortright R.D, Dumesic,R.R.J.A, Nature 2002, 418, 964.

[40] Martinez.A, Prieto, Rollan.J, J.Catal.2009, 263,292.

[41] Shen S, Hidajat K, E.Kawi, S.Adv.Mater. 2004, 16,541.

[42] Torncrona, A., J. Sterte, and J.-E. Otterstedt, Preparation of a novel fibrous catalyst support. Journal of Materials Chemistry, 1995. 5(1): p. 121-126.

[43] Shutilov, A. A.; Zenkovets, G. A.; Tsybulya, S. V.; Gavrilov, V. Y., Effect of silica on the stability of the nanostructure and texture of fine-particle alumina, Kinetics and Catalysis, 2012, 53 (1), 125-136.; Timken, H. K. C., Homogeneous modified-alumina fischer-tropsch catalyst supports, In Google Patents: 2005.

[44] https://etd.ohiolink.edu/rws_etd/document/get/osu1162323090/inline.

[45] Feng, Y., et al., Sol-flame synthesis of hybrid metal oxide nanowires. Proceedings of the Combustion Institute, 2013. 34(2): p. 2179-2186.

[46] Dinka, Peter, and Alexander S. Mukasyan. "In situ preparation of oxide-based supported catalysts by solution combustion synthesis." The Journal of Physical Chemistry B 109.46 (2005): 21627-21633.

[47] Aghayan, M.; Gasik, M.; Hussainova, I.; Rubio-Marcos, F.; Kollo, L.; Kubarsepp, J. Thermal and microstructural analysis of doped alumina nanofibers. Thermochimica Acta. 2015, 602, 43−48. DOI: 10.1016/j.tca.2015.01.009.

[48]Aghayan, M.; Hussainova, I., Fabrication of NiO/NiAl2O4 nanofibers by combustion method. Key Engineering Materials. 2016, 674, 31-34. DOI: 10.4028/www.scientific.net/KEM.674.31.

[49]Kirakosyan, K.; Aghayan, M.; Taleb, M.; Hussainova, I.; Rodríguez, M. A., Homogeneous deposition of copper oxide on mesoporous 1D alumina nanofibers by combustion approach. Proceedings of the Estonian Academy of Sciences. 2016, 65 (2) 1−4. DOI: 10.3176/proc.2016.2.06.

[50] Nazemi, M. K., et al. "Preparation of nanostructured nickel aluminate spinel powder from spent NiO/Al 2 O 3 catalyst by mechano-chemical synthesis." Advanced Powder Technology 23.6 (2012): 833-838..

[51] R. Jenkins, X-ray Techniques, Wiley, Chichester, 2000.

[52] Goldstein, Joseph, et al. Scanning electron microscopy and X-ray microanalysis: a text for biologists, materials scientists, and geologists. Springer Science & Business Media, 2012.

[53] Koo, Kee Young, et al. "Coke study on MgO-promoted Ni/Al 2 O 3 catalyst in combined H 2 O and CO 2 reforming of methane for gas to liquid (GTL) process." Applied Catalysis A: General 340.2 (2008): 183-190.

[54] Nuernberg, Giselle DB, et al. "Direct decomposition of methane over Ni catalyst supported in magnesium aluminate." Journal of Power Sources 208 (2012): 409-414.

[55] Jiang, Zheng, Xin Liao, and Yongxiang Zhao. "Comparative study of the dry reforming of methane on fluidised aerogel and xerogel Ni/Al2O3 catalysts." Applied Petrochemical Research 3.3-4 (2013): 91-99..

[56] Manukyan, Khachatur V., et al. "Ultrasmall α-Fe2O3 superparamagnetic nanoparticles with high magnetization prepared by template-assisted combustion process." The Journal of Physical Chemistry C 118.29 (2014): 16264-16271.

[57] Mehta, S. K., Ashok Kalsotra, and M. Murat. "A new approach to phase transformations in gibbsite: the role of the crystallinity." Thermochimica acta 205 (1992): 191-203.

[58] Zhu, H.Y, Riches, J.D, Barry, J.C, Chem Matter 2002,14,2086

[59] McHale, J. M., A. Navrotsky, and A. J. Perrotta. "Effects of increased surface area and chemisorbed H2O on the relative stability of nanocrystalline γ-Al2O3 and α-Al2O3." The Journal of Physical Chemistry B 101.4 (1997): 603-613.

[60] Becerra, Alberto M., and Adolfo E. Castro-Luna. "An investigation on the presence of NiAl2O4 in a stable Ni on alumina catalyst for dry reforming." Journal of the Chilean Chemical Society 50.2 (2005): 465-469.

[61] Oxy-Fuel Combustion for Power Generation and Carbon Dioxide (CO2) Capture, 14.3.4 Regeneration capability of looping materials, edited by L. Zheng.

[62] Stella, K. Christine, and A. Samson Nesaraj. "Effect of fuels on the combustion synthesis of NiAl2O4 spinel particles." Iranian Journal of Materials Science & Engineering 7.2 (2010): 36-44.

[63] Aghayan, M.; Voltsihhin, N.; Rodríguez, M.A.; Marcos, F.R.; Dong, M.; Hussainova, I., Functionalization of gamma-alumina nanofibers by alpha-alumina via solution combustion synthesis. Ceramics International 40 (8) (2014) 12603−12607. DOI: 10.1016/j.ceramint.2014.04.087.

[64] Yung, Matthew M., Whitney S. Jablonski, and Kimberly A. Magrini-Bair. "Review of catalytic conditioning of biomass-derived syngas." Energy & Fuels 23.4 (2009): 1874-1887.

[65] Seok, S.; Choi, S.; Park, E.; Han, S.; Lee, J. J. Catal. 2002, 209,6.

[66] Laosiripojana, N., Assabumrungrat, S., Appl Catal B 60, 107 (2005).

[67] P.Singh, V.K Babbar, A.Razadan, J. Applied physics, 87(2000), 4362

[68] Structural and electrical properties of certian nanocrystalline aluminates, Siby Kurien, Mahatma Gandhi University, PhD thesis.

[69] Erri, Peter, Pavol Pranda, and Arvind Varma. "Oxidizer-fuel interactions in aqueous combustion synthesis. 1. Iron (III) nitrate-model fuels." Industrial & engineering chemistry research 43.12 (2004): 3092-3096.

[70] Yablokov, V. Ya, et al. "Studies of the rates of thermal decomposition of glycine, alanine, and serine." Russian Journal of General Chemistry 79.8 (2009): 1704-1706.

[71] Schaber, Peter M., et al. "Thermal decomposition (pyrolysis) of urea in an open reaction vessel." Thermochimica acta 424.1 (2004): 131-142.

[72] Mukasyan, A. S., and P. Dinka. "Novel approaches to solution-combustion synthesis of nanomaterials." International Journal of Self-Propagating High-Temperature Synthesis 16.1 (2007): 23-35

[73] Li, Xiang, et al. "Fabrication of α-Fe 2 O 3–γ-Al 2 O 3 core–shell nanofibers and their Cr (vi) adsorptive properties." RSC Advances 4.80 (2014): 42376-42382.

[74] Hamasaki, Yosuke, et al. "Epitaxial growth of metastable multiferroic AlFeO3 film on SrTiO3 (111) substrate." Applied Physics Letters 104.8 (2014): 082906.

[75] G. M. Santosa, D. M. Silvaa, V. F. Freitasa, G. S. Diasa, A. A. Coelhob, M. Palc, I. A. Santosa, L. F. Cóticaac, R. Guoc & A. S. Bhalla, "Multiferroic Behavior of Lead-free AlFeO3 and Mn, Nb Doped Compositions", Ferroelectrics Volume 460, Issue 1, 2014.

[76] Nair, Harikrishnan S., Ramesh Kumar, and André M. Strydom. "Spin freezing in the spin-liquid compound FeAl 2 O 4." Physical Review B 91.5 (2015): 054423.

[77] Dutta, Dimple P., and Garima Sharma. "Synthesis and magnetic behavior of spinel FeAl 2 O 4 nanoparticles." Materials Science and Engineering: B 176.2 (2011): 177-180.

[78] Chirita, M., et al. "Fe2O3–nanoparticles, physical properties and their photochemical and photoelectrochemical applications." Chem. Bull 54.1 (2009).

[79] Patent CN101580279A - Preparation method of NiAl2O4 nanopowder, In Google Patents: 2004.

[80] CN 1556031 A -Burning synthesis method of NiAl2O4 spinelle powder, In Google Patents: 2005.

[81] González-Cortés, Sergio L., and Freddy E. Imbert. "Fundamentals, properties and applications of solid catalysts prepared by solution combustion synthesis (SCS)." Applied Catalysis A: General 452 (2013): 117-131.

[82] Liu, Xinsheng, Olga Korotkikh, and Robert Farrauto. "Selective catalytic oxidation of CO in H 2: structural study of Fe oxide-promoted Pt/alumina catalyst." Applied Catalysis A: General 226.1 (2002): 293-303.

[83] Jagadeesan, D.; Mansoori, U.; Mandal, P.; Sundaresan, A.; Eswaramoorthy, M. Hollow Spheres to Nanocups: Tuning the Morphology and Magnetic Properties of Single-Crystalline α-Fe2O3 Nanostructures. Angew. Chem. 2008, 120, 7799−7802. Sun, Z.

[84] Xu, X.; Cao, R.; Jeong, S.; Cho, J. Spindle-like Mesoporous α- Fe2O3 Anode Material Prepared from MOF Template for High-Rate Lithium Batteries. Nano Lett. 2012, 12, 4988−4991.

[85] Thermal Analysis TGA / DTA, ppt by Linda Fröberg (http://web.abo.fi/instut/biofuelsGS2/kursen/%C3%85A/lectures/Lectrure_Thermal%20Analysis.pdf)

[86] Marina Aghayan, Functionalization of Alumina nanofibers with metal oxides, PhD thesis, Tallinn University of Technology, 2016.

9.   ACKNOWLEDGEMENTS